

# Nansen Environmental and Remote Sensing Center



## NERSC Technical Report no. 287

### Observing sea ice ridges and deformed sea ice from satellites in the Arctic



*Example of ridges observed north of Svalbard during the Lance cruise in April 2007*


Project for Hydro Oil and Energy 2007

Contract no. 5404846

*Authors:*

*Stein Sandven, Kjell Kloster and Mohamed Babiker*

November 2007

	<p><b>Nansen Environmental and Remote Sensing Center (NERSC)</b></p> <p>Thormøhlensgate 47 N-5006 Bergen, Norway Phone: + 47 55 20 58 00 Fax: + 47 55 20 58 01 E-Mail: <a href="mailto:Stein.Sandven@nersc.no">Stein.Sandven@nersc.no</a> <a href="http://www.nersc.no">http://www.nersc.no</a></p>
---	---

<p><b>TITLE:</b></p> <p><b>Observing sea ice ridges and deformed sea ice from satellites in the Arctic</b></p>	<p><b>REPORT IDENTIFICATION</b></p> <p>NERSC Technical Report no. 287</p>
<p><b>CLIENT</b></p> <p>Hydro Oil and Energy</p>	<p><b>CONTRACT</b></p> <p>Contract no. 5404846</p>
<p><b>CLIENT REFERENCE</b></p> <p>Lars Ingolf Eide</p>	<p><b>AVAILABILITY</b></p> <p>Customer report</p>
<p><b>INVESTIGATORS</b></p> <p>Stein Sandven, Mohamed Babiker, and Kjell Kloster</p>	<p><b>AUTHORISATION</b></p> <p>Bergen, 23 November 2007</p> <p>Stein Sandven</p>



## Table of contents

<b>EXECUTIVE SUMMARY .....</b>	<b>1</b>
<b>1 INTRODUCTION.....</b>	<b>3</b>
<b>2. RIDGES AND SURFACE ROUGHNESS OBSERVATIONS FROM ALTIMETERS .....</b>	<b>6</b>
2.1 EXAMPLES OF ICESAT MEASUREMENTS OF SEA ICE .....	6
2.2 AIRBORNE LASER AND ELECTROMAGNETIC INDUCTION MEASUREMENTS .....	9
2.3 VALIDATION OF ICESAT DATA WITH AIRBORNE LASER DATA.....	11
<b>3. SAR OBSERVATION OF RIDGES AND DEFORMED SEA ICE.....</b>	<b>12</b>
3.1 THE ZIP-97 EXPERIMENT IN THE BOTHNIAN BAY.....	12
3.2 CANADIAN STUDIES WITH EM-DATA IN COMBINATION WITH SAR.....	20
3.3 EXAMPLES FROM THE RUSSIAN ARCTIC .....	24
3.4 FIELD VALIDATION OF RIDGES IN A SVALBARD FJORD .....	27
<b>4. UPCOMING SATELLITES AND NEW RETRIEVAL METHODS .....</b>	<b>29</b>
4.1 RADARSAT GEOPHYSICAL PROCESSOR SYSTEM (RGPS) .....	29
4.2. ICE THICKNESS AND ROUGHNESS FROM RADAR ALTIMETRY .....	33
<b>5. CONCLUSIONS .....</b>	<b>35</b>
<b>REFERENCES .....</b>	<b>37</b>

## Executive Summary

The objective of the study has been to assess capabilities and limitations of new earth observation satellites to detect and quantify sea ice ridges and other deformed sea ice types in the Arctic. Ridging and corresponding ice keels represent the thickest part of the sea ice cover. Detection and monitoring of ridges is therefore an important part of met-ice-ocean services to support operations in ice-covered seas.

Ridges and keels are important characteristics of the sea ice cover generated by the dynamical behaviour of sea ice forced by wind, currents and internal ice stress. Maximum thickness of sea ice is found in underneath the ridges where the keel draft is 3 – 4 times larger than the ridge height above the sea surface. The deepest free-floating ice draft observed is nearly 50 m, while the highest ridge height observed about 13 m (Wadhams, 2000). In shallow waters where the ice keels are grounded, the ridges can be even higher. The spatial distribution of ridges is highly variable, but some areas tend to have more and larger ridges due to convergence in the ice field.

On large scale ridges can be observed by laser and radar altimeter data through a surface roughness parameter that is defined by standard deviation of the surface elevation measurements along the satellite orbit. The ICESat laser altimeter has provided experimental data over six weeks periods from 2003 to 2006. These data show clearly that the area north of Greenland and the Canadian Archipelago has the highest surface roughness of the Arctic sea ice and that firstyear ice has lower roughness than multiyear ice. This is in agreement with in situ observations and with aircraft laser measurements.

On regional and local scale, satellite Synthetic Aperture Radar (SAR) images have been used to develop ridge detection methods over the last 10 – 15 years. Several studies of sea ice processes have been conducted in the Baltic Sea, the Barents Sea and Svalbard area, in

the Russian Arctic and in Canadian waters, showing that SAR can be a useful tool to detect ridges and deformed ice. The advantage of the SAR is that it can be used to discriminate areas of deformed ice from areas of level ice. Also areas with hummocks, stamukhas and individual ridges of a certain width can be identified in SAR images. SAR image cannot provide any quantitative estimate of the height of ridges. This parameter can best be measured by laser altimeter. Use of SAR images with alternating polarization and high spatial resolution (better than 10 m) is expected to improve the classification of rough ice and detection of ridges. When SAR is used in combination with laser measurements from satellite or aircraft, the detection of ridges and leads is more reliable, reducing the ambiguity of the ridge signals in SAR images. Optical images can provide detailed maps of ice ridges if the resolution is very high, such as video records from aircraft. Satellite images with very high resolution (better than 1 m) can potentially be used for ridge mapping, but images with this resolution from satellites such as Ikonos or Quickbird have not been used for such studies yet.

CryoSat-2, planned for launch in 2009, will carry a beam-limited radar altimeter with capability to map surface elevation of the sea ice. Airborne radar altimeters similar to the CryoSat-2 altimeter have been used in several campaigns to test the capability of the instrument to measure freeboard and retrieve ice thickness. The delay-Doppler Phase-monopulse (D2P) technique gives the possibility to obtain high-resolution profiles of surface elevation along the flight track. For example, flights with the D2P altimeter in combination with laser altimeters have produced high-resolution profiles across ridges and leads.

New SAR systems with polarimetric capability to produce SAR images with resolution down to 3 m will improve ridge observations compared to the present SAR images from RADARSAT and ENVISAT. Previous studies with polarimetric SAR from aircraft and space shuttle suggest that use of multi-polarisation SAR will be useful for observation of ice surface topography, but more quantitative studies are needed to find the best methodology. The recently launched TerraSAR-X and Cosmo-SkyMed satellites and RADARSAT-2 scheduled for launch in 2008 will provide both higher resolution and multipolarisation capability.

In the next 2 – 3 years, the possibility to map and quantify sea ice ridges and other local scale ice features will be significantly improved when data from CryoSat radar altimeter can be used in combination with high-resolution SAR and optical images.

# 1 Introduction

Sea ice deformation can be defined on three characteristic scales. Large-scale deformations with dimensions of the order of 100 km and more are determined mainly by external forces (internal forces are mostly balanced). Medium-scale deformations (10-20 km) are associated with the block structure of ice fields and determined by external as well as internal forces. Small-scale deformations (average diameter of single ice floe) are caused by interaction of individual ice floes (internal forces) and can be described in terms of a few basic deformation processes. During the passage of anomalous atmospheric-pressure fields, the internal forces in the sea ice field present one of the most hazardous conditions for constructions and ships in the sea-ice field.

Large scale deformation processes play the fundamental role in determining the distribution of ice thickness, which in itself controls heat and moisture fluxes between the ocean and atmosphere (Maykut, 1982). On a large scale, despite of discontinuities (cracks and fractures), the ice cover can be treated as continuous medium. That allows to apply well-developed rheological models to relate large scale deformations and internal forces. A realistic sea ice rheology must include the following general properties of sea ice cover (Hakkinen, 1987):

- a) on large scale ice cannot support tension - opening occurs with nearly no stress;
- b) with high compactness ice will resist more compression and shearing than with low compactness;
- c) thick ice resists deformation more than thin ice;
- c) the higher the compression is, the more ice will resist it (strain hardening).

Two different approaches were used to derive large-scale rheological properties (strength, viscosity coefficients) of sea ice cover based on mechanics of basic deformation processes. The first one is based on linking the amount of energy consumed in basic compressive processes (rafting and ridging) to the large scale strength of the pack ice (Rothrock, 1975).

Ridging and rafting occurs in sea ice when winds, currents or internal ice stress generate convergence in the ice field (Fig. 1).

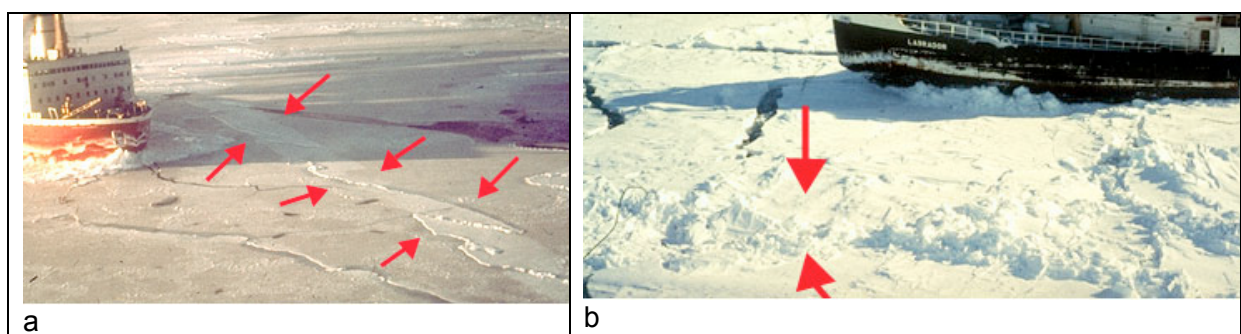


*Figure 1. Photographs of ice rafting (a) and ridging (b) in Canadian ice-covered waters. Courtesy: Canadian Ice Service.*

The largest ridges often occur near land or islands where sea ice is piled up at the shallow sea floor. The spatial distribution of ridges compared to undeformed ice is shown in the vertical video picture to the left. Typical height of ridges is from 0.5 - 2.0 m. Extreme ridge

heights of more than 10 m can occur when ice is pushed against a shore or is grounded in shallow water.

Pressure ridging is an accumulation of ice blocks which protrudes both above and below abutting ice flows. When two floes collide or squeeze together, great pressures can develop at points of contact. If the ice is unable to resist the stress, failure occurs. The result is an accumulation of blocks localized along a few points of contact or in a long ribbon. The latter is often related to the compression of thinner and, therefore, weaker ice formed in a lead system between two larger floes. Ridging is common for the thick ice categories (level ice thicker than 1 m). The compressive forces causing ridge formation are balanced by the buoyancy of the ice blocks and inertial and elastic forces developing in the ice plate. The horizontal distribution of ridges is often characterized as ridge areas with many ridges with different height, width and orientation. The largest ridges often have a preferred orientation while smaller ridges can have a more random orientation. Ridges are also characterized by the vertical dimension which is typical 0.5 – 2.0 m above the level ice (sail height) and 2 – 5 m below sea level (ice keels). Examples of ridges are shown in Fig. 2.

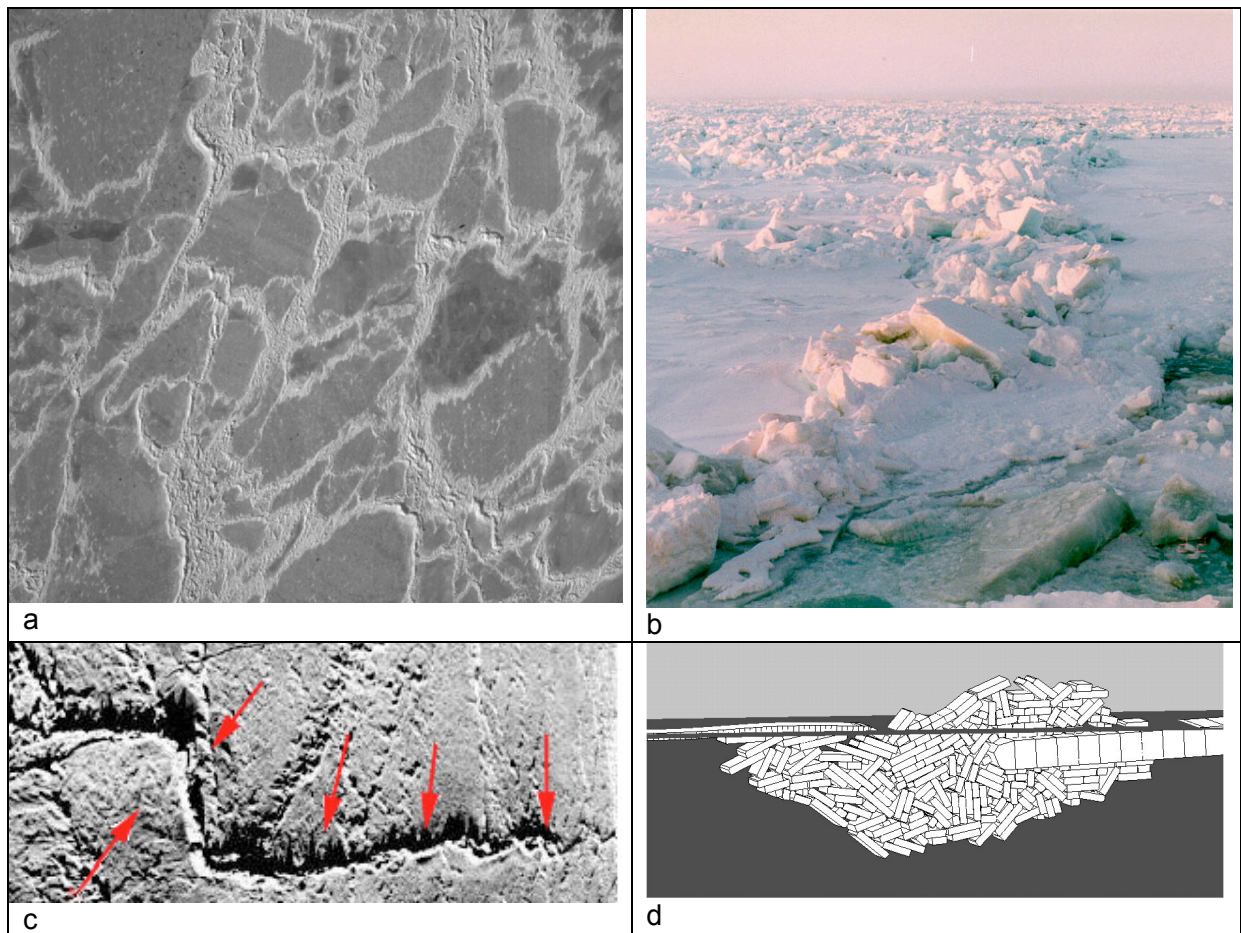
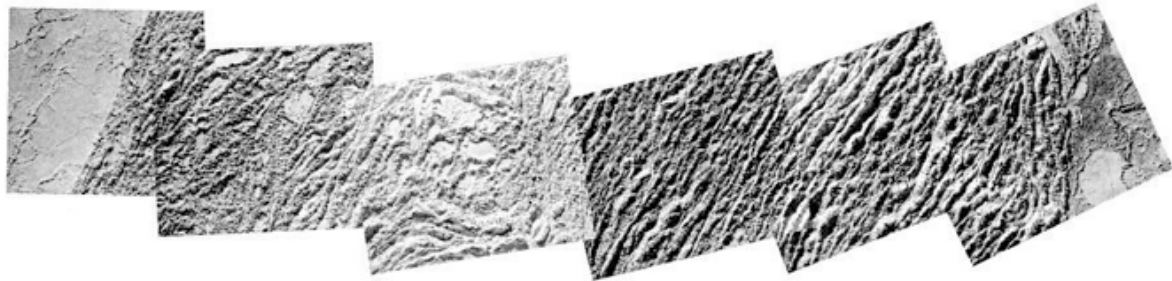


*Figure 2. (a) vertical photograph taken from a helicopter showing ridge distribution in the Bay of Bothnia, where the level ice is grayish and the ridges are shown as the bright line structures. The size of the area is about 1 by 1 km; (b) photograph of an area with heavily ridged firstyear ice taken from an icebreaker plowing through the ice; (c) aerial photograph of a dominant ridge with 2-3 m sail height, as indicated by the shadow from a low sun angle (from Kovacs, 1971); (d) illustration of the vertical profile of a ridge with sail height and keels.*



When ice deformation and ridge formation is spread over a larger area a hummock field is formed. Hummock fields most often consist of chaotic rubble of randomly dispersed block structures and ridges. Sometimes hummock fields can take on rather uniform overall appearance. Examples of hummock fields are shown in Fig. 3.



a



b



c

Figure 3. (a) Aerial photograph composite of a hummock field where the ridges have a preferred orientation; (b) photograph of a large stamukhas field (grounded ridges) from the Caspian Sea with height of about 15 m, provided by Agip KCO; (c) picture of hummock field in the Beaufort Sea provided by H. Eicken.



In shallow waters the keels of ridges can be stuck in the ground. When ice continues to be pushed against grounded keels, ridges can grow to heights above 10 m, as shown in the photograph from the Caspian Sea (Fig 3b). The result of this process can be the formation of ice islands or ramparts of hummocked ice. This phenomenon is called *stamukhas*.

## 2. Ridges and surface roughness observations from altimeters

### 2.1 Examples of ICESat measurements of sea ice

ICESat was launched in January 2003 as the first laser altimetry mission to provide large-scale mapping of the Arctic Ocean. ICESat carries the Geoscience Laser Altimeter System (GLAS). This instrument consists of two channels, at 1064 nm and 532 nm, the longer wavelength of which is used for surface altimetry. With a beam width of 110 mrad and a pulse rate of 40/s, it samples the Earth's surface from an orbit with inclination of 94° with footprints of 70 m in diameter spaced at 170 m intervals (<http://icesat.gsfc.nasa.gov/>).

One of the objectives of ICESat is to provide estimates of sea ice thickness, a key parameter of interest to the sea ice and climate communities. As laser altimeter observations of the sea ice cover are relatively new, the geophysical utility and limitations of these sea ice observations need to be investigated. Kwok et al (2006) have shown that ICESat elevation samples along the tracks over the Arctic Ocean can be used as a large-scale measure of sea ice roughness. Figure 4 shows the spatial pattern of the standard deviation of detrended ICESat elevations over a 25 km moving window for three winter periods (February – March).

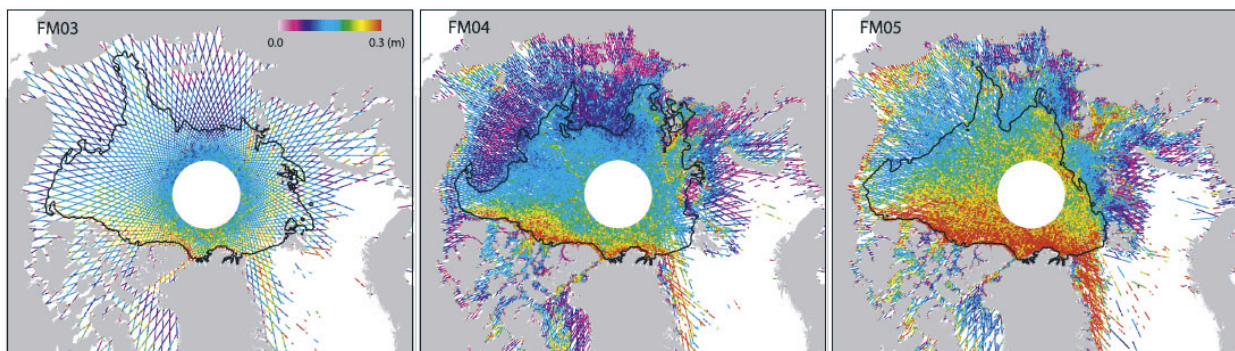


*Figure 4. The maps show ice surface roughness at 25 km length scale from the IceSat laser altimeter data for three winter periods: February - March 2003 (left), 2004 (middle) and 2005 (right). The roughness measure is the standard deviation of ice surface elevation for each 25 km segment. The maps are composed of data from all orbits where data from cloud-obscured measurements are removed. The footprint of each laser measurement is about 70 m and the distance between each measurement point is about 400 m along the satellite orbit. The black line shows the extent of multiyear ice from scatterometer data. The maps show clearly that the thickest and most heavily ridged ice is found north of Greenland and the Canadian Archipelago. It also shows that the firstyear ice has generally lower roughness than the multiyear ice. Ref. R. Kwok, 2006.*

The approximate range of roughness is from several centimeters to 30 cm. Overall, the ice cover is roughest north of Ellesmere Island and Greenland (> 30 cm), less so over much of

the MY ice cover of the central Arctic (15 cm), and smoothest in the seasonal ice zone (<10 cm). Except for FM05, the transition in roughness from the seasonal ice zone to the perennial ice zone (PIZ) can be clearly seen. The boundary between the two zones (the black contour in each figure) is derived from QuikSCAT: a Ku-band scatterometer with spatial resolution of the order of 10 km [Kwok, 2004]. Distinct differences in the backscatter from firstyear (lower backscatter) and multiyear (higher backscatter) ice in the scatterometer fields are used to delineate the two zones, shown by the black line in Fig. 4.

Even though the radar scattering cross section is dependent on more than just surface roughness, the correspondence between the changes in surface roughness and backscatter in the transition from the multiyear to the firstyear ice zone is noteworthy.

Kwok et al (2006) have examined the seasonal differences shown in Figure 5 where seasonal and year-to-year differences in ice surface elevation are shown for multiyear and firstyear ice areas. The magnitude of the differences between the February/March and October/November surveys are not far from that of 12 cm [Warren et al., 1999], suggesting that snow cover can explain most of the difference in elevation between autumn and winter.

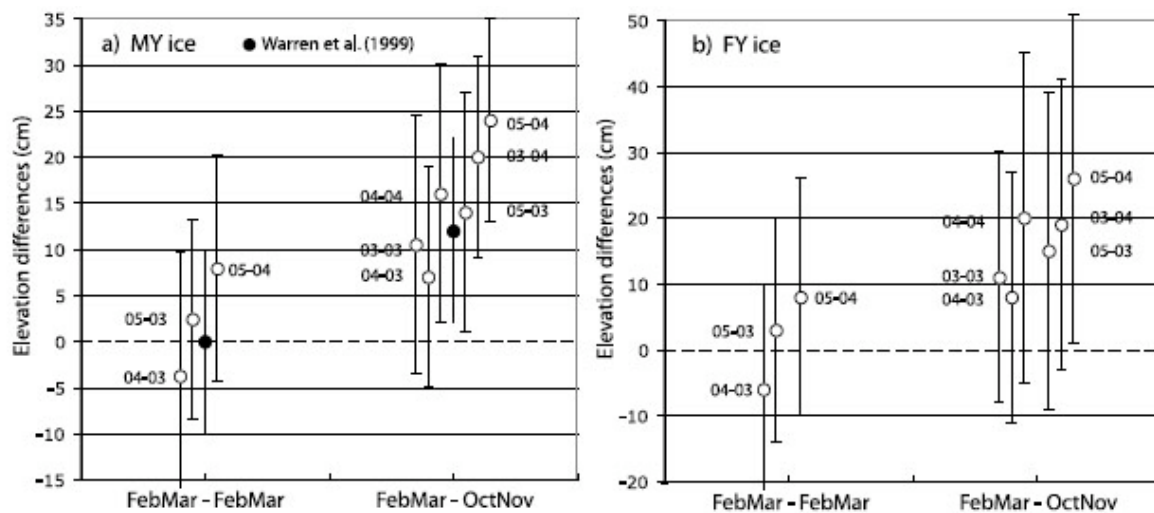


Figure 5. Difference in ice surface elevation between monthly mean values for February, March and April for 2003, 2004 and 2005 and between Feb-Mar and Oct-Nov for the same years. The figures show that the Feb-Mar ice is 10 - 20 cm higher than the Oct-Nov ice for both MY and FY ice.

In addition to studying statistical roughness and elevation changes over large areas, it also possible to identify individual ridges or ridge zones in the IceSat data. As shown in Figures 6a and b, ridges or ridge zones can be seen as distinct peaks/spikes in ICESat profiles. The two examples are from coastal Alaska and Siberia where large shear and pressure ridges are usually found. Because of the GLAS footprint size compared to the width of ridges (meters), these spikes (>0.5 m) in elevation are probably due to returns from multiple ridges rather than from an individual ridge. Whether these are due to single or multiple ridges, they appear as long linear features in SAR imagery with higher radar backscatter than that of the surrounding ice.

In the past, it has always been thought that these features were associated with ridges

[Vesecky et al., 1990], but we believe that this is the first observed correlation between spikes in surface elevation and SAR backscatter. This is complementary to the linear relation between the draft of ridges (from sonar measurements) and radar backscatter observed by Melling [1998]. The higher radar backscatter from ridges can be attributed to the following factors: (1) the lower salinity and density, and higher porosity (due to weathering) enhancing volume scattering and (2) the orientation of a certain fraction of surface facets of the piled up ice blocks toward the radar and reducing the local incidence angles. Consequently the backscatter energy of ridges is typically higher than the surrounding level ice.

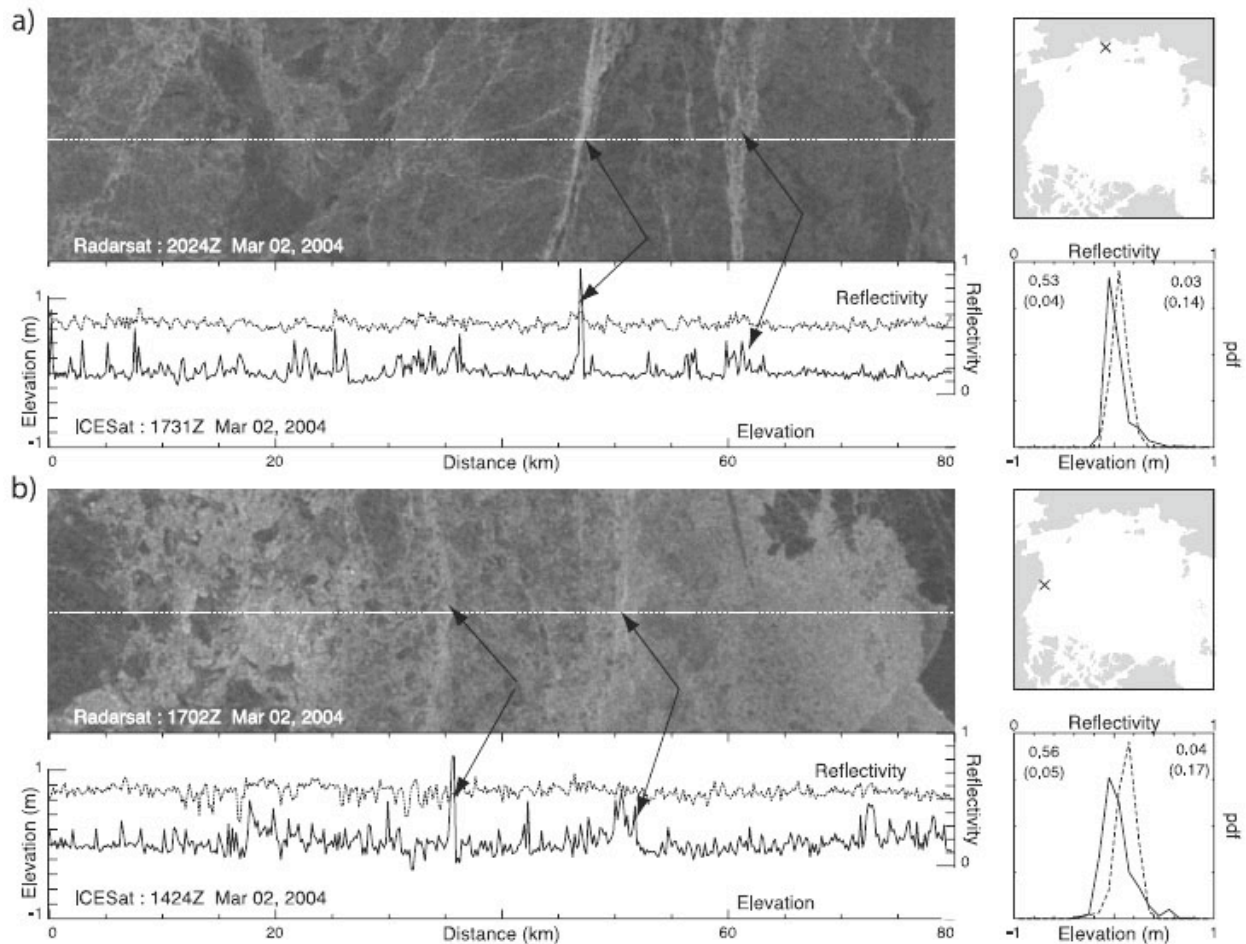


Figure 6. (a, b) Two examples of near-coincident RADARSAT and ICESat data takes over sea ice with ridges marked by arrows in the SAR images. In both examples, the ICESat track (white dashed line) and the second RADARSAT image are separated by less than 3 hours. The direction of flight is from left to right. The time separation between the ICESat and RADARSAT overflights can be computed from the date/time on the plots. The crosses on the maps mark the location of the 80 km profiles of ICESat elevations (solid) and reflectivity (dashed). Mean elevations of 25 km have been removed. Distributions of elevation and reflectivity of the samples are shown in the bottom right panel; mean and standard deviation of elevation/reflectivity are shown on the top right/left (Kwok et al., 2006).

## 2.2 Airborne laser and electromagnetic induction measurements

In recent years the helicopter-borne Electro-magnetic induction instrument (the EM-bird) has been used extensively for measuring sea ice thickness and surface roughness, including ridges. Good experience in using the EM-bird has been built up in particular at the Alfred Wegener Institute (AWI) and Bedford Institute of Oceanography in Canada.. The EM-bird used at AWI operates at 3.68 and 112 kHz. The size of the bird is relatively small (length 3.4 m, weight 100 kg), and therefore operable from icebreakers and any helicopter with an external load hook. The ice thickness retrieval is based on an electromagnetic measurement of the height of the EM– Bird above the water surface, which coincides with the ice underside. The distance from the EM-bird to the ice surface is measured by a laser altimeter. The height of the bird above the ice surface is subtracted to obtain total (ice plus snow) thickness. Key to an accurate estimate of ice thickness is the transformation of the EM signal to a distance to the water surface., which involves knowledge about water and sea ice salinity.

The laser altimeter included in the EM Bird can be used independently of the EM measurements to obtain information on surface roughness and ridge statistics. Originally, there was no DGPS extract the surface roughness profiles. However, the bird altitude variations can also roughly be removed by a combination of different high- and low-pass filters. While this does not allow computation of absolute values of surface elevation, the small scale roughness on scales of some ten meters remains unaffected. Figure 7a shows typical profiles of surface and bottom profiles of sea ice.

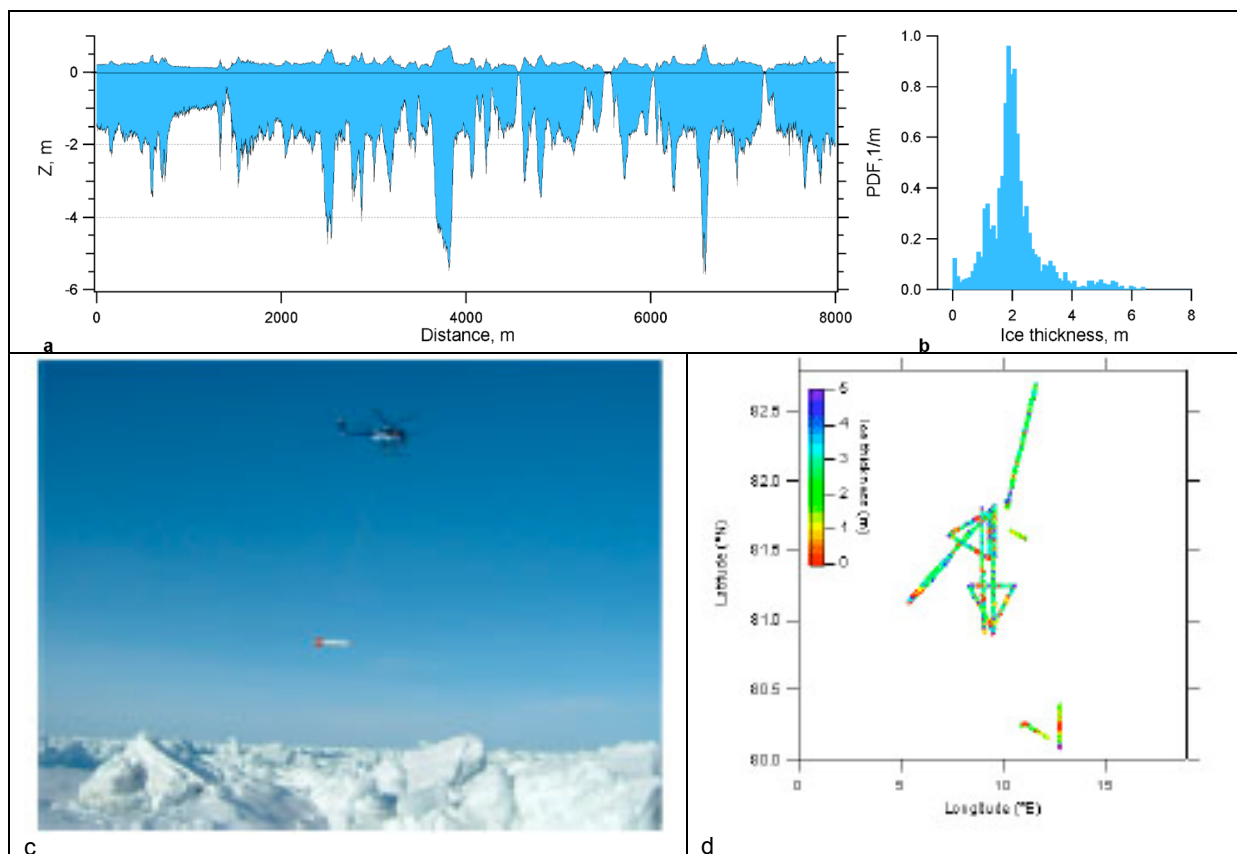


Figure 7. (a) Example of profile of ice thickness and ice surface derived from electromagnetic induction measurements from helicopter EM-bird; b) ice thickness distribution function estimated from the profile data (courtesy C. Haas); (c) photograph of the EM-bird operated from low-altitude; (d) Ice thickness along the HEM flight tracks in the Fram Strait performed during Polarstern Ark 19 cruise in 2003.



The Danish National Space Centre's laser scanner system has been used from a Twin-Otter from Air Greenland to measure sea ice elevation in several field campaigns in recent years. The system consists of the laser scanner, several precise geodetic GPS receivers and inertial navigation instrument (INS). Basic observation by the laser scanner is the range between the instrument and the surface of the snow layer on top of the sea ice. From this the surface elevation is found using information about the instrument platform (in the aircraft) position and attitude measured by the GPS and INS equipment. The measurement method is illustrated in Figure 8 a.

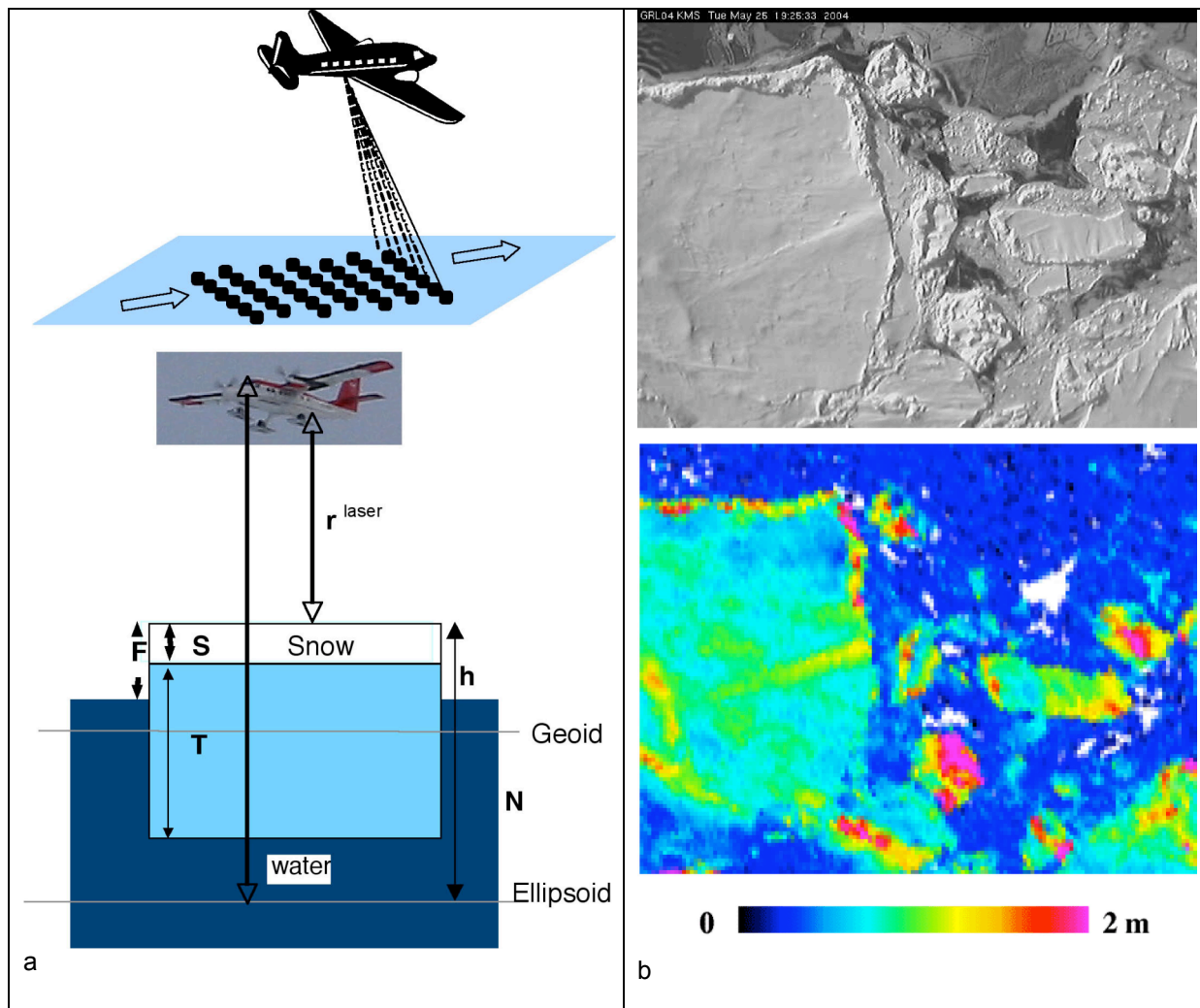


Figure 8. (a) Airborne laser scanner measurement principle. The scanning laser measures the distance to the surface of the snow layer on top of the sea ice and to the open water between the ice floes. The distance is relative a reference geoid; . (b) The lower image shows an ice freeboard image from scanning laser, where dark blue is thin or open water, while ridges with up to 2 m freeboard are yellow – red, and the upper image shows the same area observed by vertical video camera. Note that the smaller ridges around the edge of the floes and variable height within each floe can be quantified in the laser data. The size of the area is about 100 by 100 m.

From the observed surface elevations the sea ice freeboard,  $F$ , is determined by lowest-level filtering where the elevations are referred to the local sea level [Hvidegaard and Forsberg,



2002]. The sea ice thickness can then be estimated from the freeboard observations using a ratio,  $K$ , between the freeboard and the thickness expressed as,  $T=K \cdot F$ . With total ice and snow thickness  $T$ .  $K$  is an empirical relation between snow and ice thickness and density.

Examples of scanning laser image of sea surface of the results is shown in Figure 8 b where the lower image is surface elevation from the laser and the upper image is a video picture of the same ice area. The laser image shows detailed height of the ice floes, the ridges and the thin ice between the floes. The resolution of the laser image is less than 1 m, allowing detailed mapping of the ridges.

During the SITHOS project 2002-2006, many airborne scanning laser data of sea ice were collected in the area north of Greenland and in the Fram Strait (Fig. 9 a). An example of scanning laser strip is shown in Fig. 9 b where ridges are identified in the elevation data as yellow-red signature in contrast to the undeformed, level ice with blue signature.

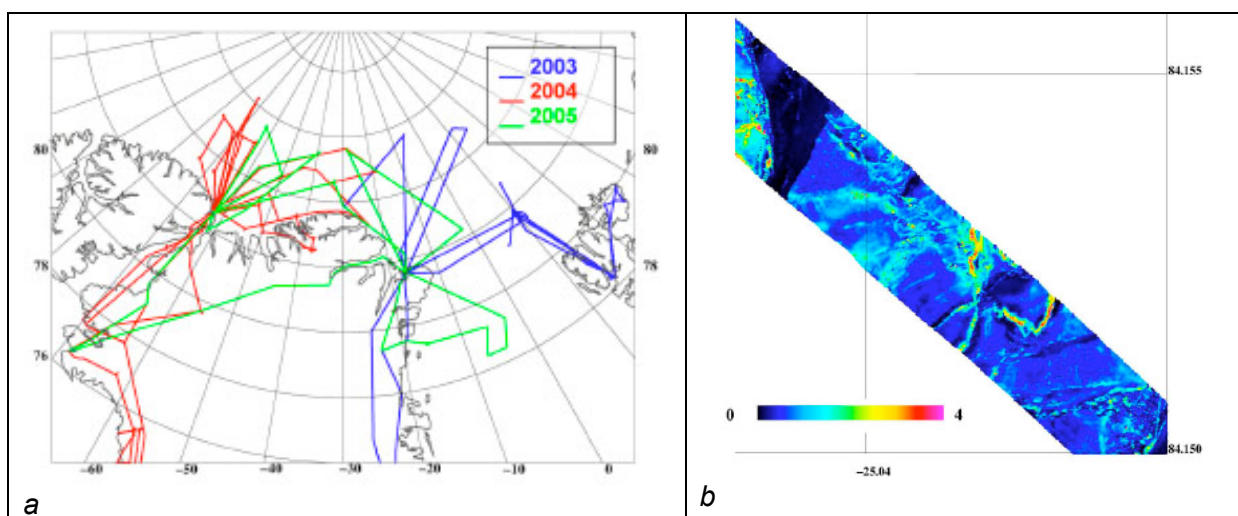
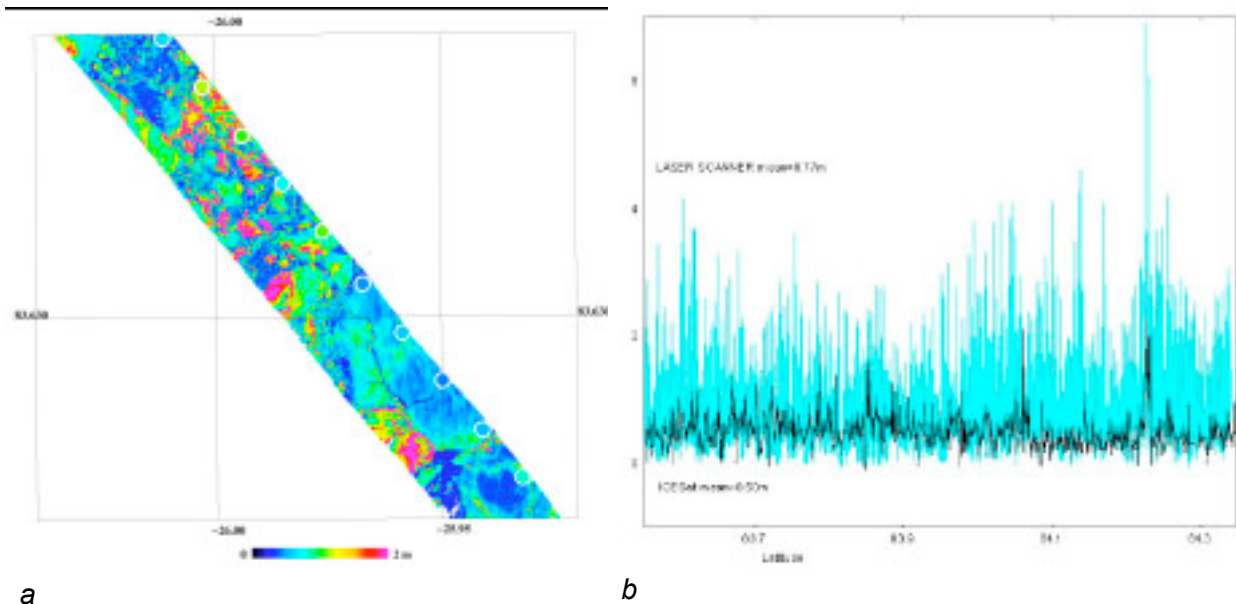


Figure 9. (a) Airborne laser scanner survey flight tracks in the SITHOS project 2003-2005; (b) Image stripe of laser scanner freeboard height in meter. The swath width is 150 m. The ridges are clearly seen as yellow-red features, while level ice is blue and thin ice/leads are dark blue (Sandven et al., 2006).

## 2.3 Validation of ICESat data with airborne laser data

Validation of ICESat laser data of surface elevation have been conducted during airborne campaigns with scanning laser and GPS data north of Greenland. During the 2004 campaign two flight lines were flown nearly coincident with ICESat sub-tracks, as shown in Fig. 10. To the left laser swath data is overlaid with ICESat point measurements and to the right a longer profile of freeboard elevations from laser scanner, in blue, and ICESat, in black, is seen. The lower resolution and larger footprint of ICESat compared to the airborne data results in different profile data, as shown in Fig. 10 b. Many individual ridges are not sampled by the ICESat data, but larger ridge areas in contrast to level ice are well mapped by the ICESat data.



*Figure 10. (a) Laser scanning swath example of freeboard heights north of Greenland with coincident ICESat height shown as white circles; (b) profiles of airborne lidar in blue and corresponding ICESat in black.*

### 3. SAR observation of ridges and deformed sea ice

#### 3.1 The ZIP-97 experiment in the Bothnian Bay

Satellite SAR observations of sea ice is an essential method in the studies of local ice cover deformation and mesoscale ice dynamics. During the ZIP-97 field investigation in the Bothnian Bay in March 1997 SAR images from satellites were obtained in combination with several other ice observations. The satellite data, which included SAR and optical images, were used to study both basin wide as well as intermediate and local scale ice dynamics. The most important data were the Synthetic Aperture Radar (SAR) images from ERS-2 and RADARSAT. The SAR data were used for ice type classification, ridge mapping, identification of floes, leads, shear zones, drifting ice and fast ice. Repeated satellite images could also provide estimates of ice motion to be compared with GPS drifters. The main advantage of satellite data is the possibility to get synoptic images of large ice areas and synoptic ice motion estimates. The satellite data used in ZIP-97 are presented in a technical report (Sandven et al., 1997).

ZIP-97 offered the first opportunity to study sea ice in the Baltic Sea with both ERS and RADARSAT images as well as high resolution Russian satellite images. Several cloudfree days during ZIP-97 made it possible to use the optical images from the Russian satellite Resurs-O1, with pixel size down to 40 m. From RADARSAT different modes of images were used, where the highest resolution was 6 m. The radar images are used in combination with aerial photographs and with high-resolution optical images from the Resurs satellite. Such comparisons are useful for evaluation of the ability of SAR images to classify ice types, and to identify ridges and other small ice features which reflect the dynamic nature of the sea ice.

During the period from 22 February to 18 March, a total of 9 SAR images (or stripes) were available from the ERS-2 and RADARSAT satellites in near real-time. Also 4 images from two optical instruments onboard on the Resurs O1-N3 satellite and two Okean SLR images were obtained after the experiment. After processing at NERSC in near real-time, most of

the SAR images were sent out to the ZIP-97 Headquarters on Hailuoto Island by fax and/or by digital file transfer. These image products had reduced spatial resolution and were contrast enhanced. At the Headquarters, the image files were displayed, further enhanced, hardcopied and used for planning of field investigation.

The satellite information is necessary for obtaining quantitative ice parameters on large and intermediate scale, and to use this parameters in the coupling to local scale observations from the field experiment. The ice velocity estimates and ice deformation maps from SAR data will be used to validate the ice model simulations of ice drift, shear zones, convergence zones and ridge formation. The ScanSAR Narrow mode image of 17. March was the first wideswath SAR image covering practically the whole Bothnian Bay (Fig. 11).

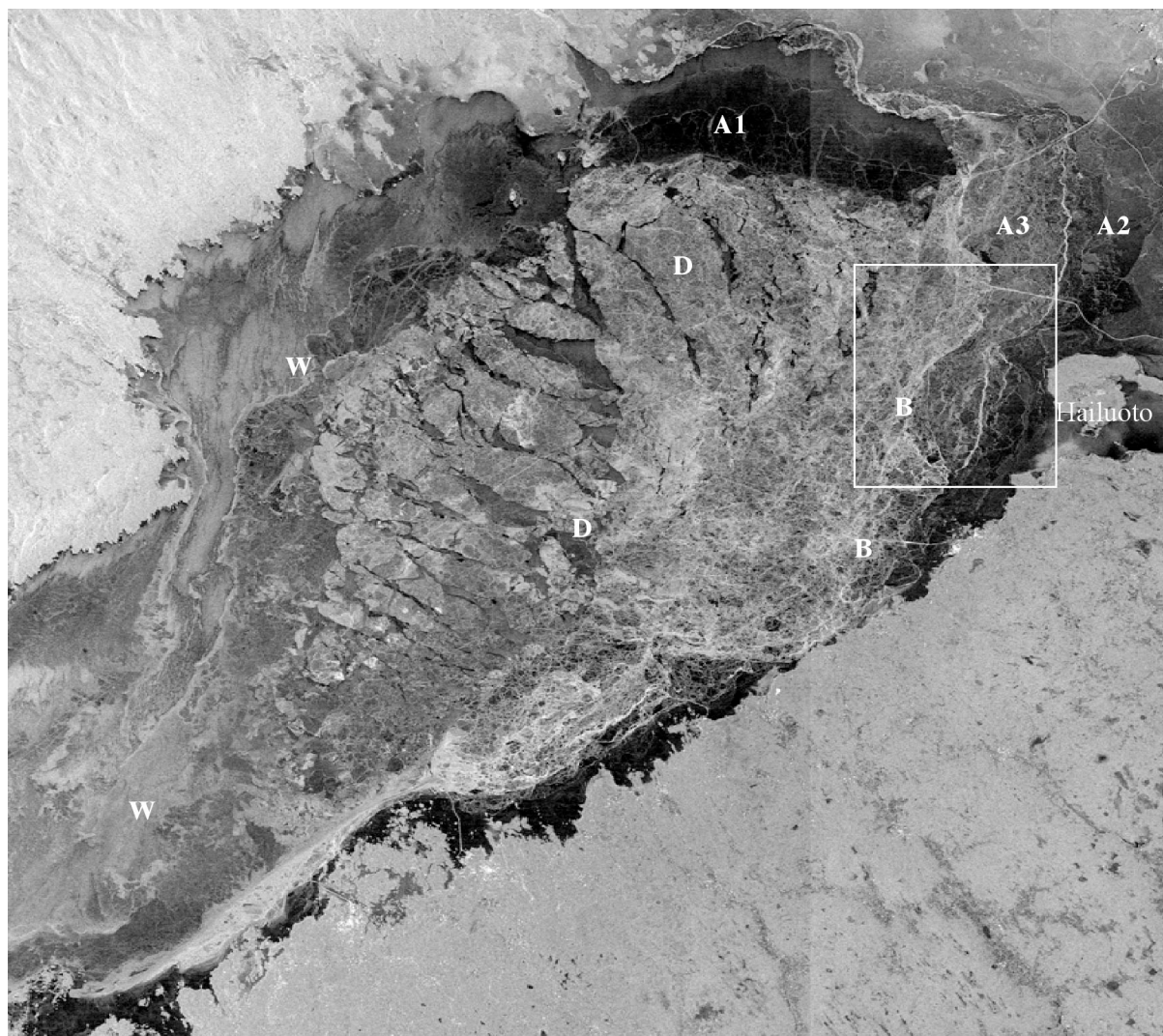


*Figure 11. RADARSAT ScanSAR image with 300km swath width, obtained on 17 March 1997 during the ZIP'97 experiment in the Bothnian Bay. The white frame, which indicates the key area investigated in the experiment, show the location of the blow-up image in Fig. 13. The main ice characteristics indicated by the white letters are described in the text. Copyright © Canadian Space Agency.*

The image shows the following main features. Areas denoted “A” represent several stages of fastice along the northern and eastern sides of the Bothnian Bay, shown as relatively dark areas. The fastice consists of large areas of level ice and various amounts of surface roughness, shown by different grey tones, and individual ridges shown as bright line features.

Area “A1” is thin level ice which has been formed in the last 2 -3 days in the lead created as the main icepack drifted southwards. Area “A2” is older and thicker fast ice which started to develop in December containing ridges which are grounded many places. The thickness of this ice was around 70 cm. Area “A3” is a zone which earlier in the winter ice had ice moving in response to variable wind forcing, but was fastice in March. This zone has more ridges and rubble ice than “A1” and “A2”. The thickness of level ice, observed by in situ observations, varied between 50 and 90 cm, while the maximum thickness observed in a ridge was 7 m.

“B” is the transition zone between fastice and drifting ice further west. The SAR image shows more bright features in this zone compared to the fast ice. These features are caused by numerous ridges and rubble fields. This is the area where GPS drifters were deployed in ZIP-97. The drifters were used to quantify the mesoscale ice velocity .

“D” marks the drifting ice in the western part of the Bothnian Bay, which started to move southwards immediately after the onset of northerly winds in the period from 13 to 15 March. The drifting packice field was diverging, creating leads between clusters of floes or congested ice areas which moved like a solid body. The leads were refrozen and became covered by thin level ice which appears dark in the SAR image. The air temperature in this period varied between - 6° and -12°C. “W” indicates areas of predominantly open water and scattered new ice in the western part of the Bothnian Bay and in the Bothnian Sea.

The Fine-resolution RADARSAT images obtained west of Hailuoto on 10 and 13 March were used to study the transition zone between fastice and the drifting ice which moved slightly towards east in this period. The area covered by both Fine-resolution images is shown in Fig. 12.



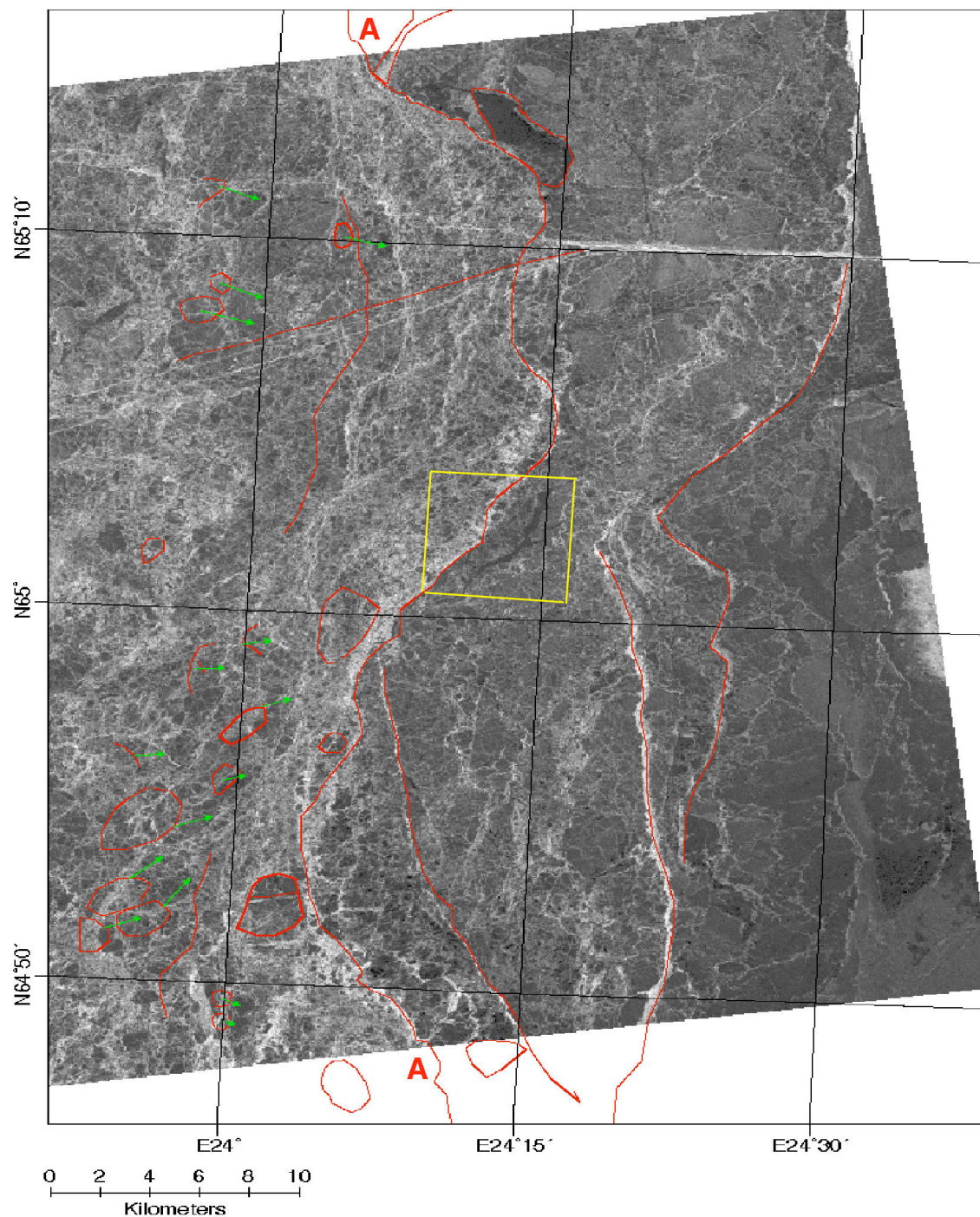
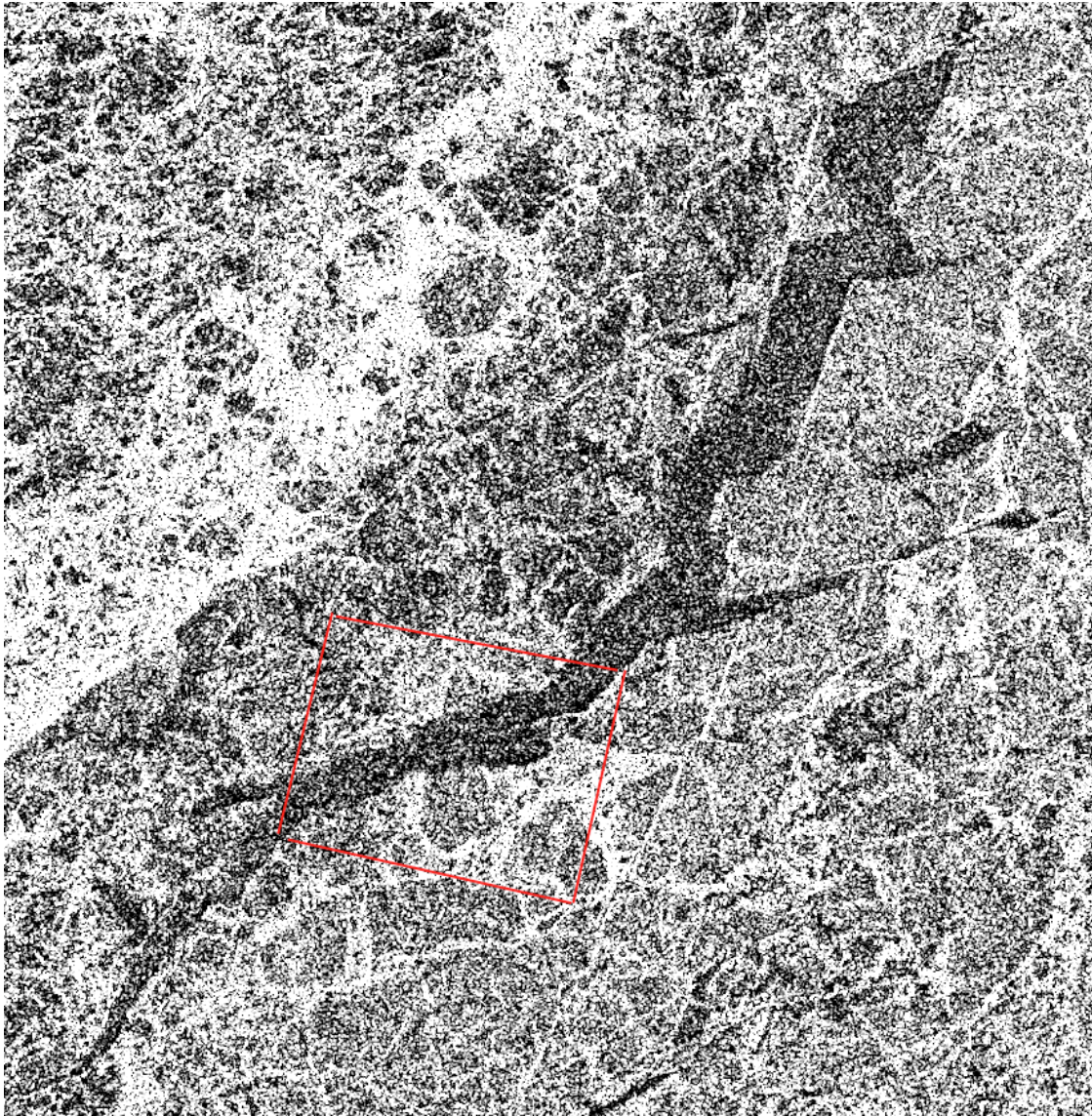


Figure 12. The image shows the area covered by RADARSAT Fine-resolution image on 10 and 13 March in the area west of Hailuoto. The line marked "A" indicates the border between the fastice on the eastern side and the drifting ice on the western side. The red lines and polygons enhance the main ridges and features in the image used to determine the ice motion (indicated by the arrows). The yellow box shows a subset of the Fine Resolution image presented in higher resolution in Fig. 13.





*Figure 13. Subimage of a RADARSAT Fine Resolution image, covering 12.5 by 12.5 km, taken just west of Hailuoto on 13 March. The image has pixel size of 12.5 by 12.5 m and is averaged from the full resolution image with pixels of 6.25 by 6.25 m. The red box shows location of a vertical photograph taken by helicopter, shown in Fig. 14a.*

Accurate geolocation has been achieved by assuming that the major ridges running north-south between 24°15' E and 24°30' E are stationary. Comparison of features in two images from 10 and 13 March, obtained by laying them on top of each other in the image analysis system, shows that the ice west of the line denoted "A" running north-south in the centre of the image moved eastwards up to two km in three days, corresponding to a mean speed of  $0.008 \text{ ms}^{-1}$ .

Optical images give a different, but complementary compared to SAR images. Both helicopter images (Fig. 14) and satellite optical images (Fig. 15) were used to investigate the surface properties of ice during ZIP-97. Since most of the ice in the Hailuoto area was snow-free, the optical images showed level ice to be dark. Ridges appeared bright due to the fact that snow had accumulated in the ridges because of wind accumulation in the previous days and weeks. Figure 14 shows two examples of vertical photographs taken from



helicopter flying at 3000 feet altitude. Comparison between the optical image and the radar image shows very similar patterns of ridges (bright line features) and level ice areas (darker, grayish signature). Fig 14a shows level ice and ridges surrounding the lead visible in the SAR image in Fig. 13, while Fig. 14b shows fast ice with many ridges west of Hailuoto.

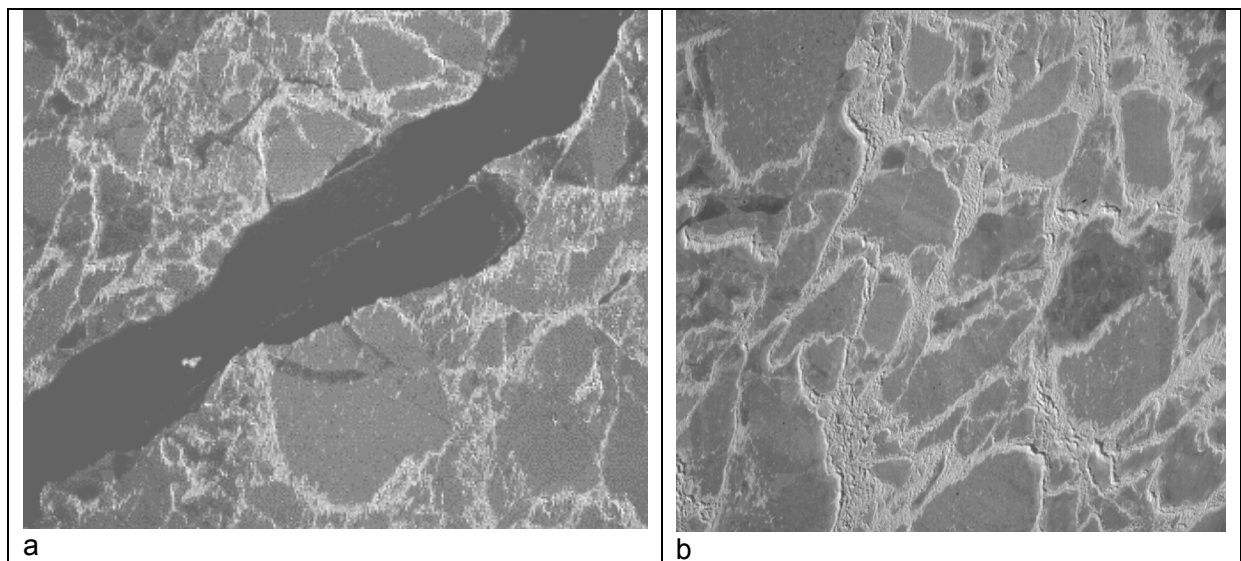


*Figure 14. Aerial photograph showing characteristic patterns of ridges and level ice in an area of about 1 by 1 km, where (a) is from the lead identified in Fig. 3 and (b) is from the fast ice west of Hailuoto. Such photographs were used to validate observations from optical and radar satellites. Courtesy: J. Haapala, FIMR.*

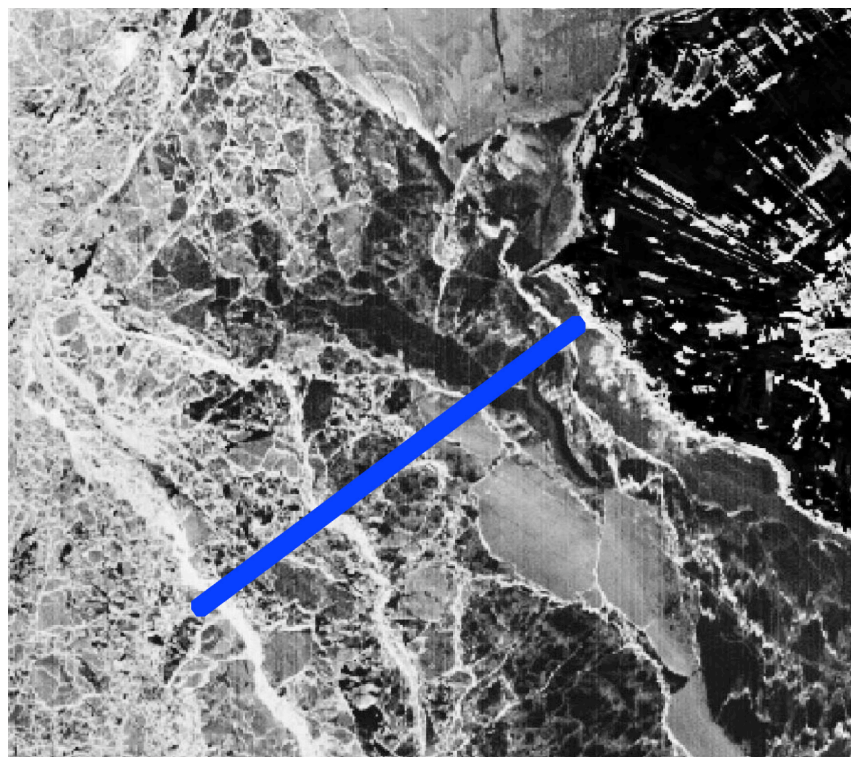


*Figure 15. Subset of a Ressurs MSU-E image covering about 15 by 15 km of the Hailuoto area, obtained on March 18 1997. The blue line is the 10 km long profile with laser measurements from aircraft shown in Fig. 16*

The MSU-E sensor is a multichannel high-resolution scanning imager onboard the Russian Resurs-01 satellite, providing images with resolution of about 40 m in 45 km wide swaths. A sub-set of the optical image obtained on 18 March is shown in Fig. 15, where the bright line structures are ridges, similar to what is seen in the aerial photographs in Fig. 14. The level ice has various grey tones, reflecting bare ice with little or no snow cover.

Laser data are used in combination with satellite data to study the surface topography of the sea ice. Airborne laser profilometer measurements were obtained in the northeast sector of the Bay of Bothnia during the field experiment to quantify ridge sail heights and ridge density. Aerial photographs were obtained for identification of ridges, ice floes, ice types and snow cover. The photographs, in addition to the in situ observations, were used for validation of the satellite observations. Profiles of SAR backscatter, optical radiation and laser height measurements from an east-west section just west of Hailuoto are shown in Figure 16. The laser profiles show the ridge heights directly, while the satellite data also include the effect of rafting, snow cover and other small scale features at the surface.

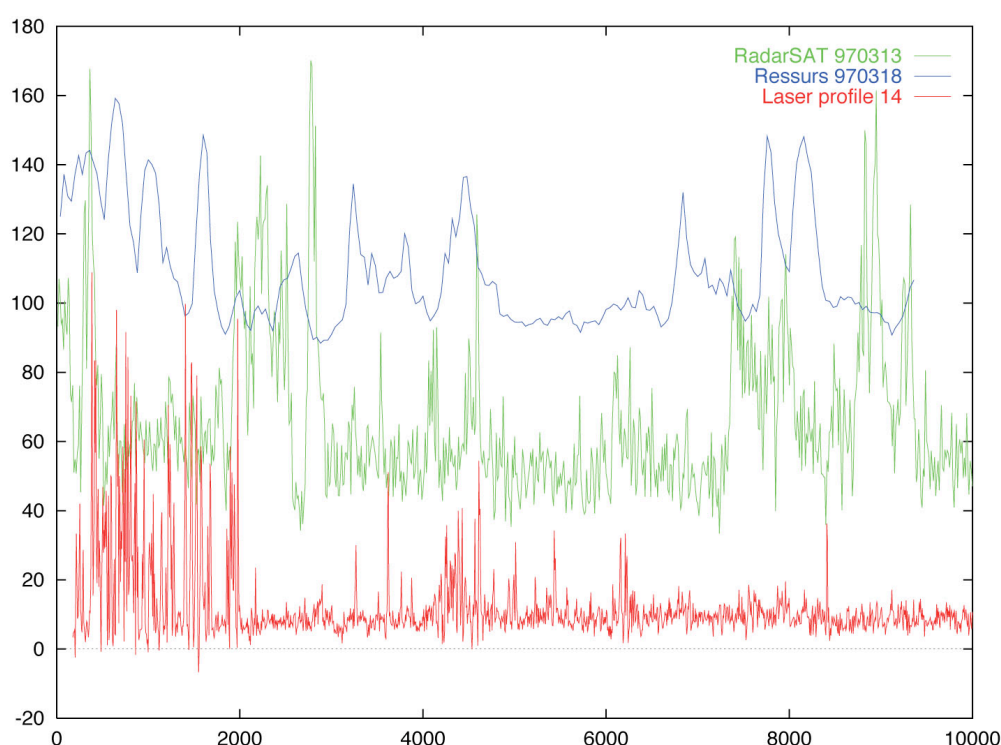


*Figure 16. Example of profiles of MSU-E optical image from Resurs-01 (upper graph), RADARSAT SAR (middle graph) and airborne laser measurements (lower graph) taken in a 10 km long section just west of Hailuoto during ZIP-97. The laser data are provided by Mikko Lensu. The horizontal axis is in meter, and the vertical axis is in cm showing the height measurements from the laser. The vertical scale of the satellite data is arbitrary.*

During ZIP-97 a number of in situ measurements of ridge sizes were made based on observations in the SAR images. Of particular interest was the study of how Fine-Resolution RADARSAT images with pixel size down to less than 10 m could identify various ridges in the area around Hailuoto. A subimage of the Fine-Resolution image obtained on 10 March has been used to superimpose a selection of positions where in situ measurements were made in the period from 11 to 21 March (Fig. 17). Examples of ice characteristics in the 17 areas shown in Fig 17 are:

1. Level ice with ridges not higher than 50 – 60 cm. Small scale roughness of order 1 cm. 70 – 80 % of the ice area is snowfree.
2. Level ice with small ridges, less than 50 cm. Some of the level ice was like a mirror without any small-scale roughness
3. Area of generally rough ice with typical roughness scale of 20 – 30 cm
4. Large area of ridges not higher than 1 m. Thickness of floes in the ridges is typical 20 cm.
5. 70 – 80 % of the area is covered with ridges, where ice thickness is about 40 cm. The bright line just west of the area is 100 % covered with ridges.
6. A ridge which is 2 – 3 m high and 5 m wide, surrounded by rough ice in 20 – 40 % of the area
7. Ice floe dominated by many bands of rough ice which are 1 – 2 m wide and with height of roughness from 10 – 30 cm
8. Many small floes of level ice with ridges between floes of 1 – 2 m height
9. Individual ridge of height up to 2.5 m and width of 40 – 50 m.
10. Undulating ice near land which is stuck to bottom with 20 – 30 cm height differences
11. Level ice without snow
12. Rough ice with height scale of 20 – 30 cm
13. Level ice with ridges in the neighborhood of 1 – 1.5 m height and 5 m width
14. At the border between level ice and rough ice further south
15. At the boundary between level and rough ice with height scale of 20 cm and width of about 1 m
16. A single hummock 100 m long and 10 – 20 m wide and up to 4 m high
17. A large hummock of 5 m height and more than 100 m in diameter

Such in situ observations are compared qualitatively with the backscatter from SAR images.

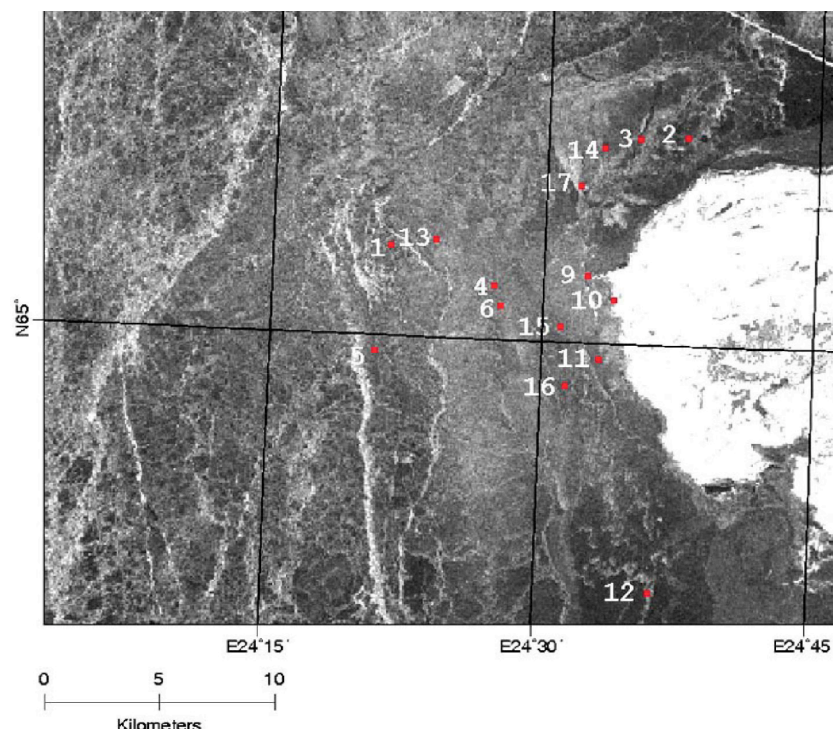
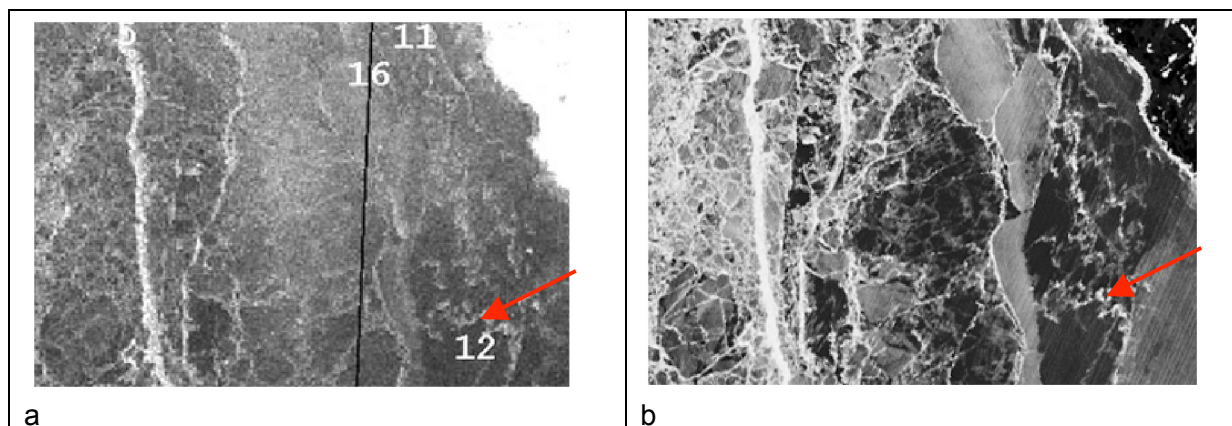


Figure 17. A subimage extracted from the RADARSAT Fine-Resolution image of 10 March 1997 with pixel size of 75 by 75 m, after averaging the original pixels of 12.5 by 12.5 m. The points (1 – 17) show the location of a selection of in situ ice observations. A subset of the area is shown in Fig. 18 where both SAR and optical images identify ridge patterns.





*Figure 18 (a) Subset of the SAR image in Fig. 17, where the red arrow showing rough ice with height of 20 – 30 cm; (b) the same area mapped by the optical satellite image from Fig. 15. The ridges are well-defined in the optical image because snow is accumulated in the ridges and rough ice areas, while the level ice is mostly snow-free.*

The study during the ZIP-97 experiment has demonstrated that SAR images from satellites (RADARSAT and ERS-2) can be used to describe and map several ice types, ice roughness categories and ice features such as fastice, leads, ridge and other ice phenomena in the Bothnian Bay. For observation of ridges and other forms of rough ice, SAR images showed good capability to detect features. In situ observations were compared with SAR signatures showing that ridges as small as 20 – 30 cm can be detected both in SAR images and optical images if the extent of the ridge area is of order 10m or more (Fig. 18, point 12). But it is not yet clear to what extent quantitative measurements of ridges of different sizes can be obtained from SAR data. Airborne laser measurements were used to provide actual height and distribution of ridges, whereas SAR can mainly be used for mapping of areas with ridges and rough ice and discriminate them from areas of level ice. High-resolution optical images also showed good correspondence with the SAR images and could be used for mapping of ridge and level ice.

In a follow-up project from 2002 - 2006, IRIS, many aspects of sea ice ridging in the Baltic Sea were studied, including observing techniques, modeling, forecasting and decision support for ice operations (IRIS Synthesis Report, 2006). More information is available at <http://www.tkk.fi/Units/Ship/Research/Iris/Public/>.

### **3.2 Canadian studies with EM-data in combination with SAR**

In April-May 2004, a field survey of sea-ice thickness and surface roughness using helicopter-borne sensors was conducted over the eastern Beaufort shelf as part of the Canadian Arctic Shelf Exchange Study (CASES). Sea ice thickness and roughness profiles were collected with an electromagnetic-laser system mounted on the front of a helicopter, and video data were frame-grabbed in real-time using a downward-looking video camera. The upper graph of Fig. 19 shows ice thickness and roughness data collected with the fix-mounted electromagnetic (FEM)-laser system plotted along a 20 km line leading up to and including the thin first-year ice region. The snow-ice surface roughness measured with the laser altimeter increased at locations where the EM sensor detected deep ice features, as expected for ridges (Peterson et al., 2006).



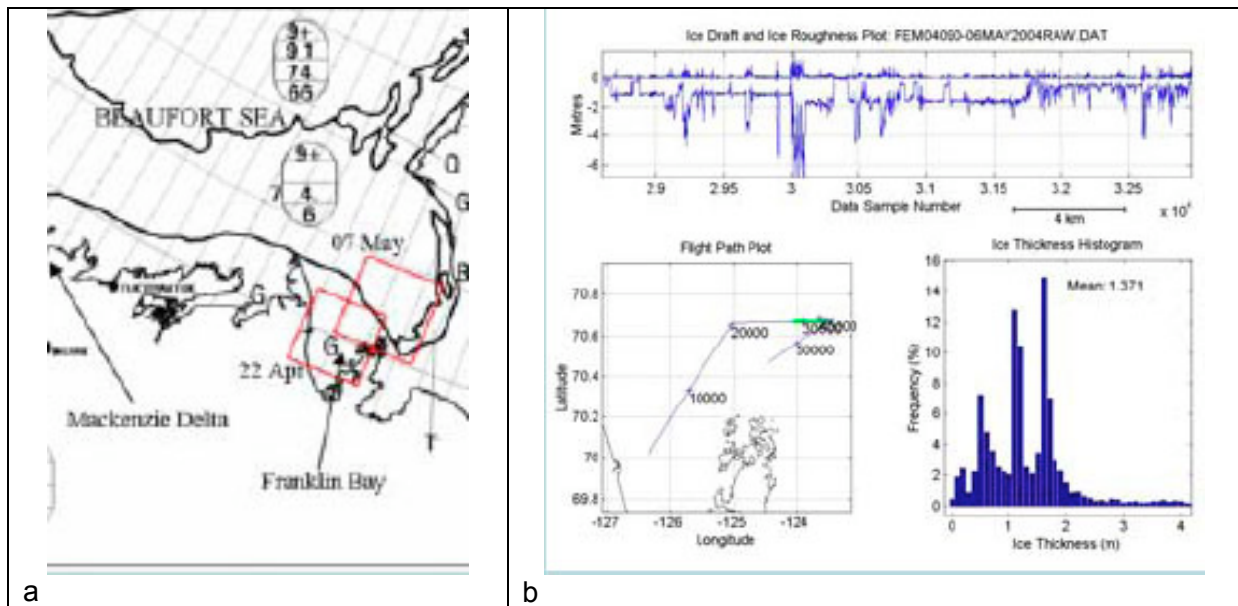


Figure 19. (a) Part of the ice chart (Canadian Ice Service) for May 15, 2004 showing landfast or compact ice (10-tenths concentration) in Franklin Bay, mobile thick first-year ice (>9-tenths concentration) to the north, and a narrow region ("T") of first-year ice to the northeast along the eastern edge of the Bathurst polynya. The red boxes show SAR APP coverage from ENVISAT, where the image from 07 May is shown in Fig. 20; (b) Ice thickness and roughness data collected with the fix-mounted electromagnetic (FEM)-laser system along the flight line shown in the lower left map. Three regions having modal ice thicknesses of 1.1m, 1.6m and 0.5m are observed from west to east; a few refrozen leads covered with thin ice (10-30cm) are also present in the ice thickness histogram.

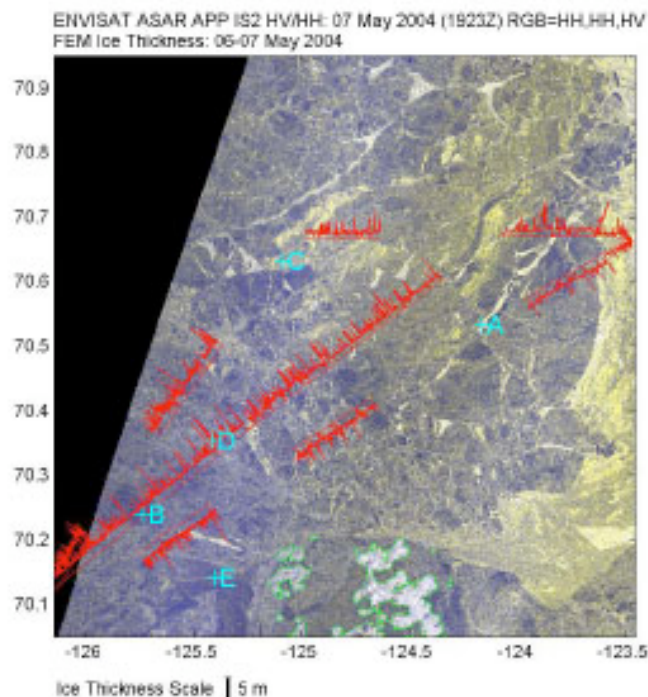


Figure 20. ENVISAT ASAR APP Image acquired on May 7, 2004 (100km x 100km, Swath IS2, HH+HV polarization) overlain with FEM-measured ice thickness profiles collected on May 6-7. Ice thickness data are plotted relative to the straight line representing the location of the flight path. © ESA 2004.

Advanced synthetic aperture radar (ASAR) images were also acquired from ENVISAT, providing dual-polarization data. The field and satellite data were collected to assess the improved capabilities of dual-polarization SAR data for monitoring sea-ice type and ice-surface topography, and ultimately for developing and validating ice-classification algorithms based on SAR data.

An example of an HH+HV ENVISAT ASAR alternating polarization mode precision (APP) image acquired on May 7 is shown in Fig. 20. Most of the image is within the mobile thick first-year ice area, as indicated by the presence of white-toned refrozen leads. The yellow-toned area at the right side of the image represents the area of thin first-year ice and the area south of about 70.2°N represents the landfast ice area. Ice thickness data are overlain on the ASAR image in red. Ice thicknesses of 0.2-0.3m are observed in the white-toned refrozen leads; the high radar return is due to the presence of frost flowers. Ice thicknesses of about 0.6m were observed in the yellow-toned thin firstyear ice area at the right side of the image. Uniform ice thicknesses of 1.7-2.1m are observed for dark-toned smooth level ice (e.g. "B" in Fig. 20). Higher radar backscatter is observed at "C", which represents rough-surfaced consolidated brash ice as observed in the video imagery. Higher backscatter is also observed at "D" which represents deformed thick first-year ice, where thicknesses are generally 2 m with peaks up to 10m, and the ice roughness is as high as about 4m.

Mean radar backscattering coefficient  $\sigma^0$  as a function of laser-measured ice thickness for HH and HV polarizations from the 07 May image are presented in Figure 21.

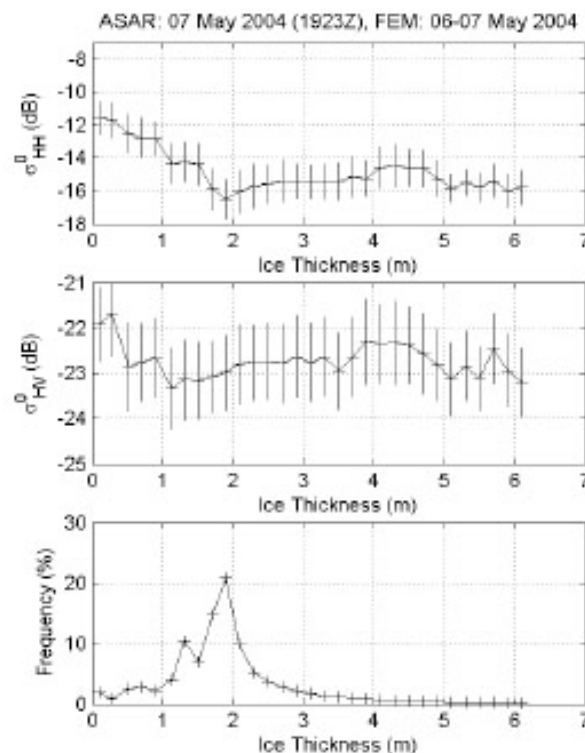


Figure 21. Mean radar backscattering coefficient  $\sigma^0$  as a function of FEM measured ice thickness for HH and HV polarizations of the May 07 image. The vertical lines represent the mean  $\pm 0.5$  standard deviations. Ice thickness frequency is shown in the bottom plot.

The frozen leads with a thickness of 0-0.4m have the highest backscatter for both the HH and HV channels. As ice thickness increases from 0.3m to 2m, HH backscatter decreases steadily to a minimum of about -16dB. However the HV backscatter decreases sharply by 1dB as ice thickness increases from 0.3m to 0.5m, and is relatively constant for thicknesses between 1m and 2m. As ice thickness increases from 2m to 4m, the HH and VV backscattering coefficients increase by about 2dB, and the HV backscatter increases by about 0.6dB (Peterson et al., 2006).

The effect of incidence angle on the backscattering coefficient was determined using six scenes covering the landfast ice area in Franklin Bay. The scenes were from swaths IS2, IS4 and IS6 and were acquired between 21 April and 10 May, 2004 from both ascending and descending passes.

In Fig. 22, the mean of the backscattering coefficient is plotted as a function of incidence angle for four targets: two areas of level ice and two areas of deformed ice, in the top three panels. For the two areas of deformed ice, the backscattering coefficients are very similar, for both the HH and VV polarizations, and the slope of the lines are -0.15 to -0.16dB/degree for the HH polarization and -0.20 dB/degree for the VV polarization. Thus the contrast between level and deformed ice is fairly constant with increasing incidence angle for level ice 1, but decreases with increasing incidence angle for level ice 2. In conclusion, deformed ice has significant higher backscatter than level ice at HH and VV polarisations, but not at HV, for all incidence angles.

An example of SAR ice type classification and thickness profiles from FEM data in Gulf of St. Lawrence is shown in Fig. 23. More information about the Canadian studies, see <http://www.mar.dfo-mpo.gc.ca/science/ocean/seaice/public.html>).

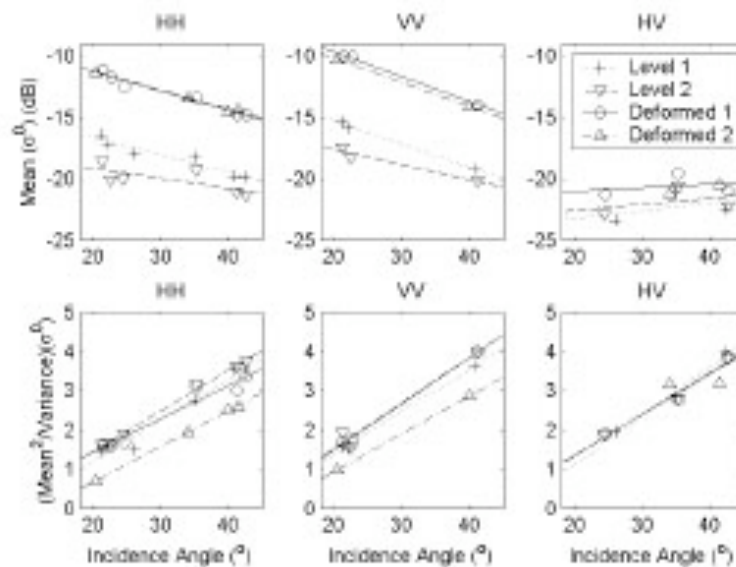


Figure 22. Backscattering coefficient as a function of incidence angle for level and deformed ice in Franklin Bay.



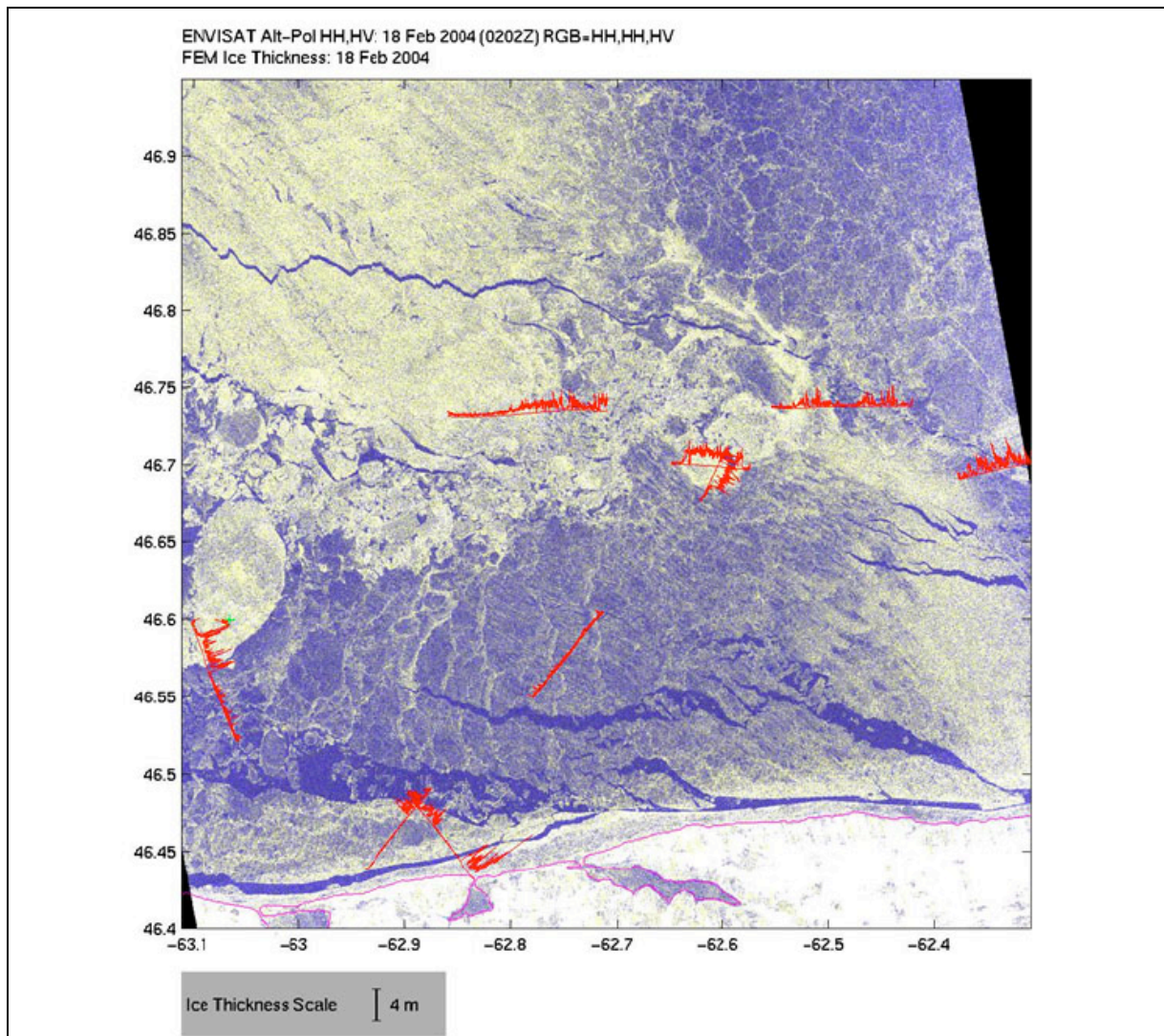


Figure 23. An example of ENVISAT ASAR AP image from February 18 2004, covering 55 x 55 km area in Gulf of St. Lawrence. The HH and HV polarisations are combined in the RGB presentation, showing medium blue as thinner thinner ice and yellow as thicker FY ice. The dark blue shows offshore leads that indicate diverging pack ice. The north shores of Prince Edward Island is indicated at the bottom. The red lines are ice thickness profiles from airborne FEM surveys. The FEM data documents that the thickness varies between the ice types present in this image.

### 3.3 Examples from the Russian Arctic

In April 1998, an ice navigation experiment was conducted in the Russian Arctic as part of a research expedition with icebreaker Kapitan Dranitsyn. SAR images of the Ob Estuary were obtained and transferred to the icebreaker in near real time (Pettersson et al., 1999). The SAR images shown in Fig. 24 were used to discriminate between undeformed, level ice of thickness about 1.0 m (dark signature) and deformed ice with ridges and hummocks (bright signature). This information was used by the icebreaker to select the best navigation route in level ice, avoiding the deformed ice which was much thicker than the level ice.

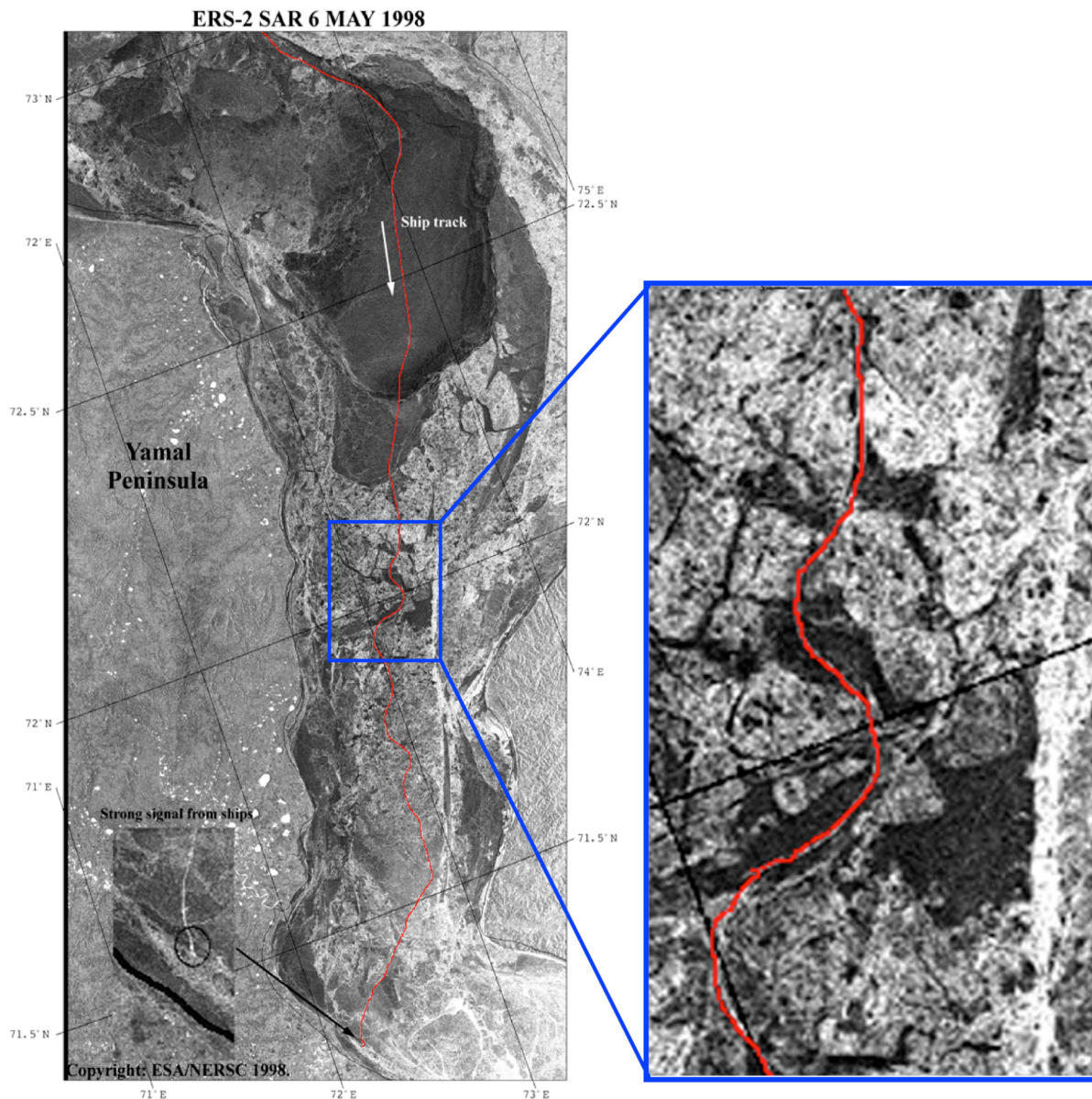


Figure 24. Left image: ERS-2 SAR image of the Ob Gulf in April 1998. The red line shows the sailing route of the icebreaker. Right image: zoom-in of the SAR image in an area dominated by deformed ice and ridges, shown as bright signature. The red line shows the sailing route following the level ice identified by dark signature.

Another example of ridge observation in the Ob Estuary is shown in Fig. 25 where ridge information in a SAR image is compared with a ship radar image obtained from an icebreaker. The features observed in both images include:

- A - level thick fast ice (ice rind)
- B - river ice zone (rotated ice floes), resulting from ice drift in fall
- C - river ice zone (rotated ice floes), resulting from ice drift
- D - tidal crack
- E - hummocks formed at the grey ice stage
- F - ridged ice zone formed at the grey ice stage



G - ridged ice formed at the grey-white ice stage, the ridges and hummocks are aged and weathered

H - icebreaker channel

This example demonstrates that many ridges are observable in SAR images.

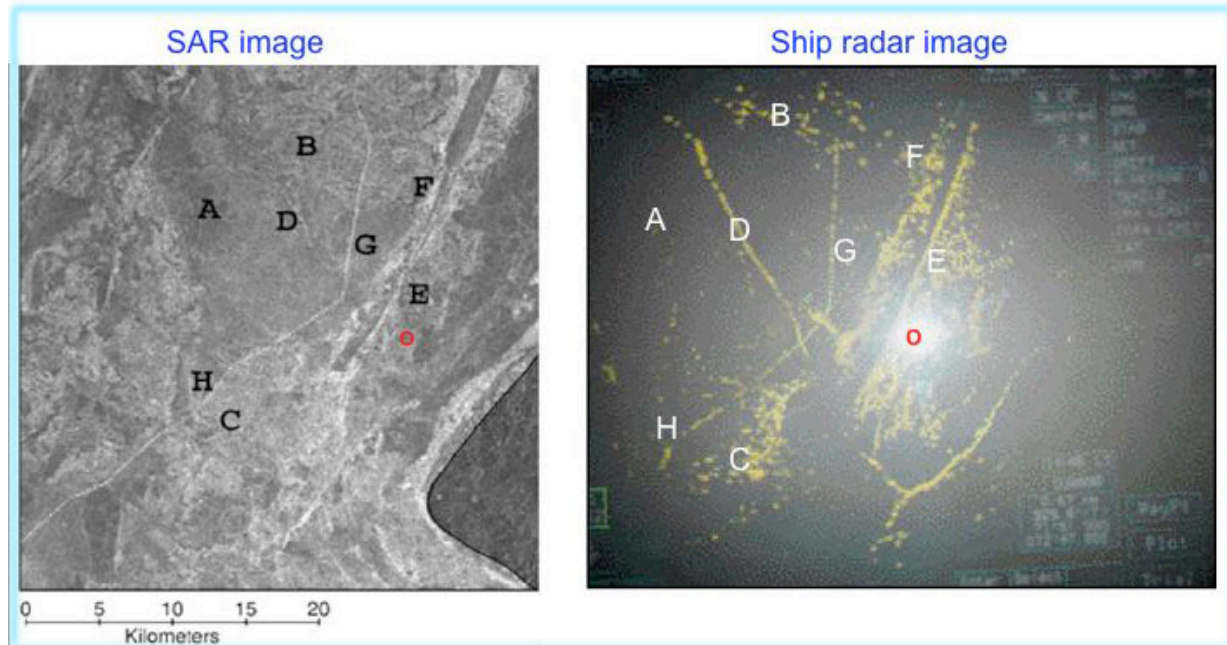


*Figure 25. Left: Subset of an ERS-2 SAR image in the Ob Estuary showing line structures indicating ridges and hummock areas. Right: the ship radar on the icebreaker (located in the red circle), provided images of ridges and hummocks with a radius of 15 - 20 km (right side). The features A – H in this image are compared to the SAR image.*

The possibilities to use SAR images to map ridges and other sea ice features of importance to ice navigation and offshore operations in the Northern Sea Route are described in the book "Remote Sensing of Sea ice in the Northern Sea Route: Studies and Applications. Praxis Springer" by Johannessen et al (2007), where results of SAR sea ice studies in the Russian Arctic over the last 15 years are presented.

High-resolution optical images from the Russian Resurs MSUE satellite can also give useful information about ridges and deformation zones in first year ice in the Kara Sea, as shown in Fig. 26. Cracks and deformation zones in fast ice near the coast are clearly visible in the image. Also level ice can be distinguished from deformed ice, which has bright signature due to snow cover, similar as the examples from the Bay of Bothnia (e.g. Fig. 15). Note that islands have important impact on the cracks in the ice which is generated due to dynamic forcing on the ice cover from wind, current and tides.



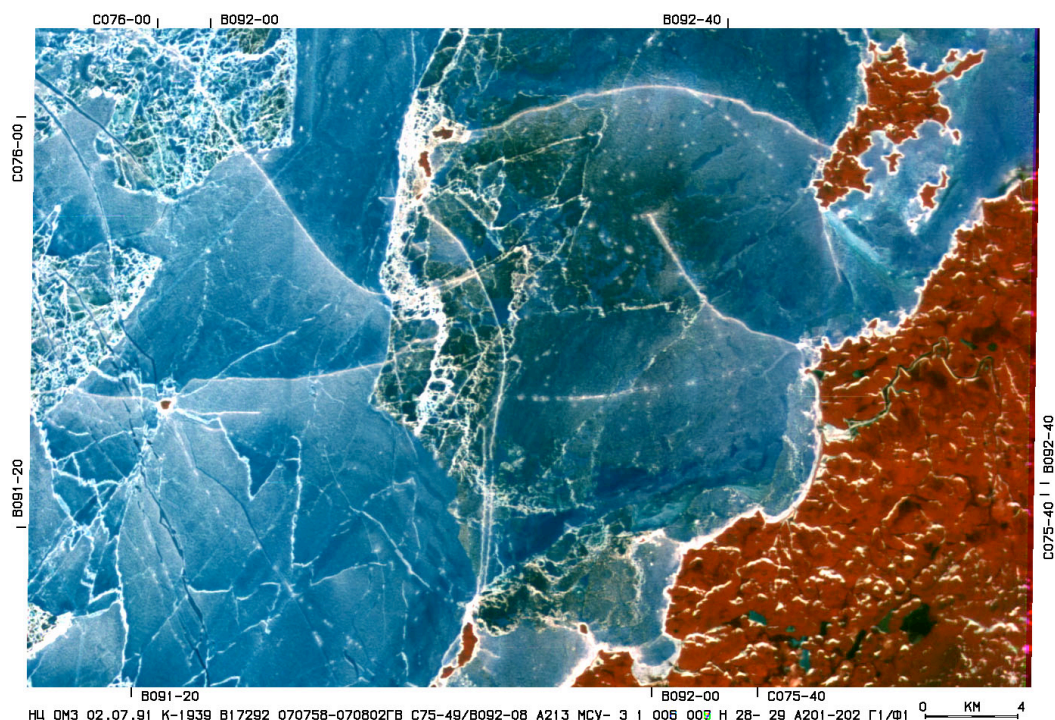


Figure 26. Optical image from RESOURS-O1 MSU-E with 30 m pixel size obtained on 02. July 1991, showing level ice (A), cracks, deformation and shear zones (B) and ridges/hummock areas/rubble fields (C). The image is presented in false colours using several optical bands. The image was obtained on 02 July 1991 in the Kara Sea along the Taimyr peninsula. Courtesy: NTsOMZ, Moscow.

### 3.4 Field validation of ridges in a Svalbard fjord

During a field experiment with RV Lance in Wahlenbergfjorden in April 2007, sea ice ridges and keels were measured and satellite images were collected in the study area (Fig. 27).

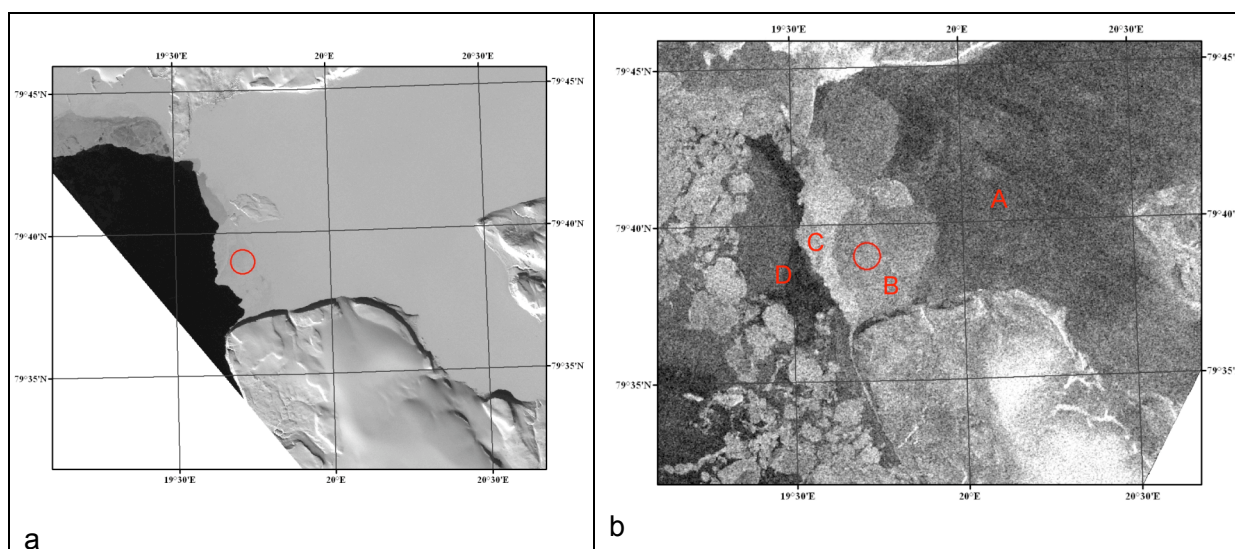
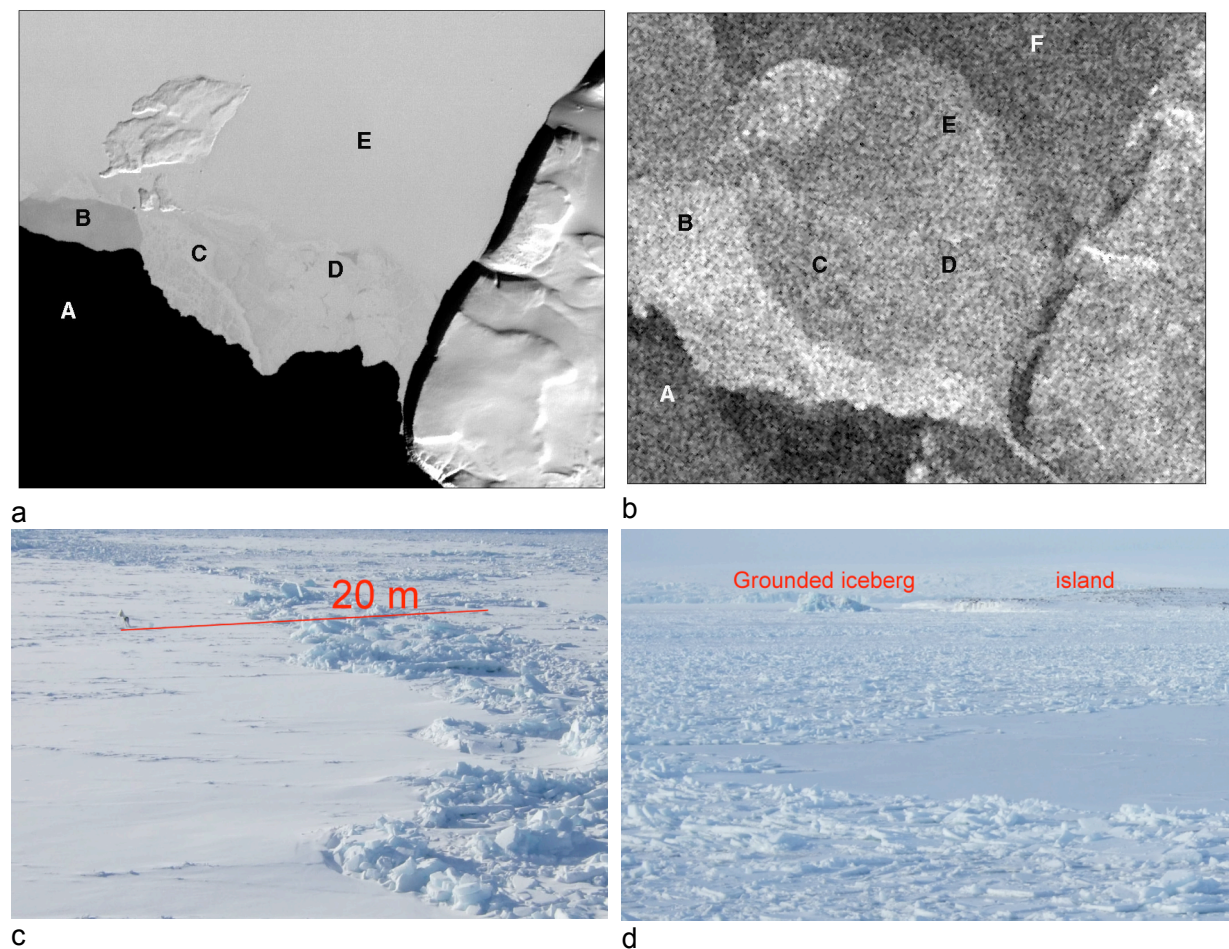


Figure 27 (a) Subset of a Landsat image 29 April 2007, indicating the location of Lance (red circle) with fastice to the east and open water to the west; (b) SAR image from RADARSAT of the same area on 23 April 2007.

The Landsat image of 29 April 2007 shows the fastice as bright signature and open water as dark signature. The red circle shows the position of Lance during the field experiment 19 - 23 April 2007. There is very little difference in the optical signature of level ice and deformed ice with ridges. SAR image of 23 April 2007 showing the same area as the Landsat image. The backscatter data can distinguish between undeformed fastice (A), fastice with ridges and hummocks (B), firstyear-ice and young ice with high roughness on 5-cm scale (C) and open water/nilas (D). Note that are C and D changed from 23 to 29 April, because easterly winds have blown the thin ice to the west, leaving open water to west of the fastice boundary

By zooming in on the details of the images it is possible to identify different types of ice surfaces, as shown in Fig. 28. The dominant ridge running in east-west direction (Fig. 28c) can be identified in the SAR image but not in the Landsat image. The SAR image from RADARAT had a pixel size of 25 m, which is too large to identify the numerous smaller ridges in the area.



*Figure 28. (a) Landsat image showing A: open water, B: young ice 20 – 30 cm thick, C: firstyear ice with rubble fields and ridges, D: firstyear ice floes with thin ice between, E: fastice; (b) SAR image showing A: open water, B: young ice, C: firstyear ice with rubble fields and ridges, D: a larger ridge extending in east-west direction can be identified as brighter signature in the SAR image, E: fastice with smaller rubbles, F: fastice without any surface roughness; (c) Photograph of the large ridge which was typical 10 m wide and 1-2m sail height; (d) photograph of the rubble field near point C, with view of the island in the upper left part of the satellite images.*



## 4. Upcoming satellites and new retrieval methods

### 4.1 RADARSAT Geophysical Processor System (RGPS)

With more systematic acquisition and access to wide swath SAR data with high resolution it will be possible to perform more detailed mapping of sea ice processes that is not feasible with coarse resolution data. From a sequence of SAR images covering the major part of the Arctic Ocean, ice drift and deformation fields can be estimated according to the approach of the RADARSAT Geophysical Processor System (RGPS) developed by Kwok (1998). For each cell where ice drift is calculated, the formation and aging of new ice as well as deformation (ridge formation) during the freezing season is followed in the time series of images. This allows determination of various stages in new and young ice whereas the discrimination between multiyear and first-year ice area is done by image classification. The age distribution of young ice can be converted to a thickness distribution using a simple empirical relation between accumulated freezing days and thickness (Fig. 29).

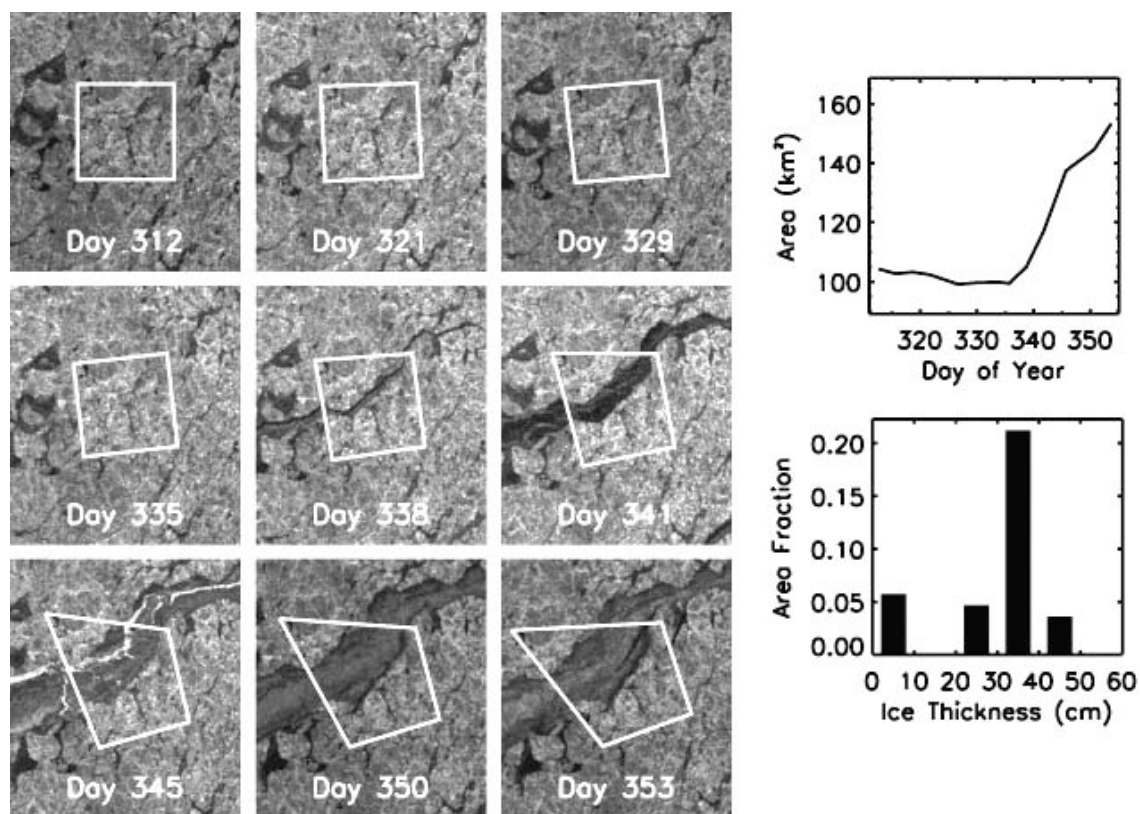


Figure 29. Example of ice drift and deformation of a grid cell of Arctic sea ice observed in a sequence of SAR images. The grid cell is initially 10 by 10 km and grows through the ice season in this case where a lead is opening up and new ice is formed. The thickness distribution of new ice is calculated as freezing progresses.

The RGPS can therefore be used to estimate the thickness distribution of ice volume produced by openings and closings of the ice cover since the beginning of the freezing season. Other products from RGPS are maps of thin ice categories and map of various Linear Kinematics Features (LKFs) derived from the ice drift vectors (Fig. 30). The LKFs include long, narrow features whether or not they contain open water, new ice, nilas,



young ice, firstyear ice, rafted ice or ridged ice. Locally, they can be created by divergence, convergence, shear, or a combination of these (Kwok and Cunningham, 2002). Examples of other RGPS products can be found at <http://www-radar.jpl.nasa.gov/rgps/radarsat.html>.

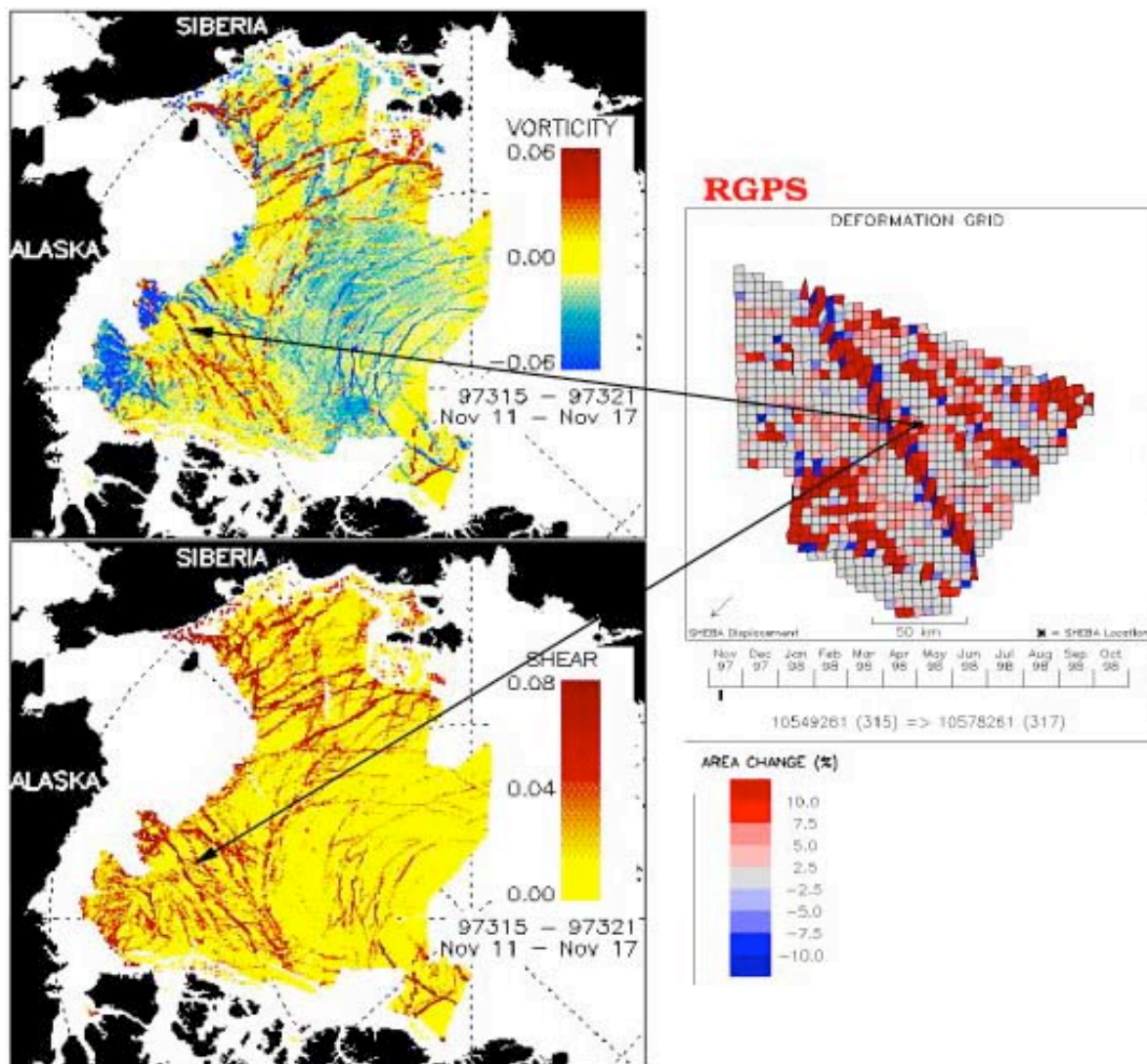


Figure 30. Sea ice vorticity and shear fields are example of Linear Kinematic Field calculated from 6 day interval mosaics of the Arctic ice cover using the deformation grids explained in Fig. 29.

The launch of RADARSAT-2, planned in 2008, will secure access to wideswath SAR data for large coverage as well as fine resolution SAR for detailed studies in smaller areas. Use of SAR data with different coverage, resolution and polarisation will provide more quantitative information about dynamical and thermo-dynamical behaviour of the ice cover throughout the year. When ice thickness data from CryoSat is combined with ice dynamic and ice type information from SAR, it is expected that new data on ice volume and fluxes can be retrieved. Sea ice services will offer more satellite based products in all ice areas both in the Northern Hemisphere and in the Antarctica.

Dual-polarisation SAR data from ENVISAT and later from RADARSAT-2 and other planned SAR missions is expected to improve sea ice classification and feature extraction (i.e. edge detection, ridge detection) and reduce some of the ambiguities and uncertainties that exist in single-channel and single polarisation SAR data. Other new spaceborne SAR systems will contribute to ice observation in the next few years, such as the L-band, polarimetric ALOS PALSAR, and the X- and L-band polarimetric TerraSAR. The possibilities to have SAR data in three frequencies (X-, C- and L-band) in combination with polarimetric capabilities offer unique opportunities to extract more information about various ice classes and ice features from SAR. An example of a three frequency composite (P-, C- and L-band) from airborne SAR is shown in Fig. 31.

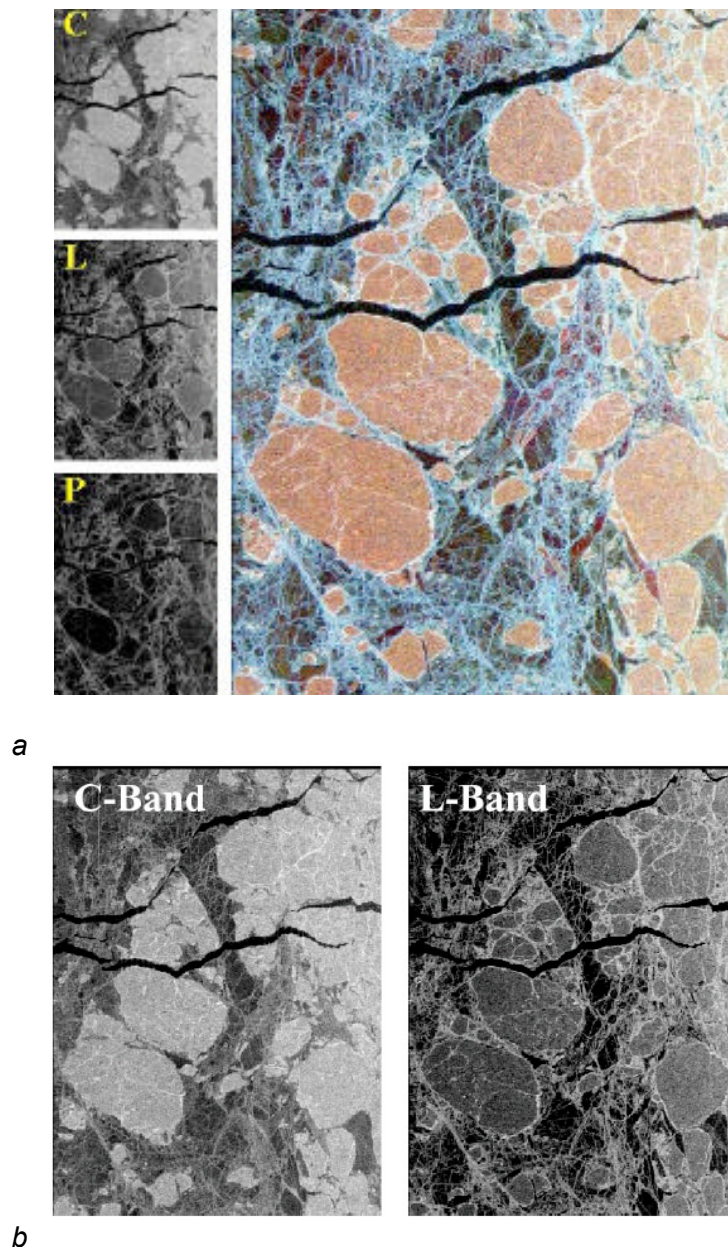


Figure 31. (a): Example of ice classification using C-, L- and P-band from the JPL airborne SAR system; (b) comparison of L-band and C-band image showing that L-band gives better enhancement of mechanical deformation features compared to C-band (Courtesy JPL).

By use of polarization ratio HH/VV compared to VV in C-band SAR images it is possible to classify deformed firstyear ice from other ice types, as shown by Erikson et al., (2001) in Fig. 32.

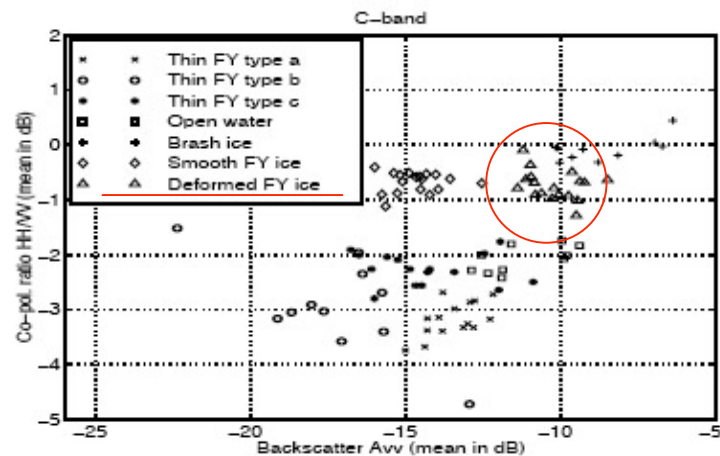


Figure 32. Analysis of  $s_0$  from SIR-C SAR data over Antarctic sea ice, showing the possibilities to discriminate between ice types and surface roughness using multipolarisation SAR images. Deformed firstyear ice can to some extent be separated from other ice types in the diagram (red circle), but more robust classification will require more than one SAR frequency, as shown in the JPL SAR data in Fig. 31.

Sea ice classification methods using polarized SAR data that can extract ridges are presented in Fig. 33.

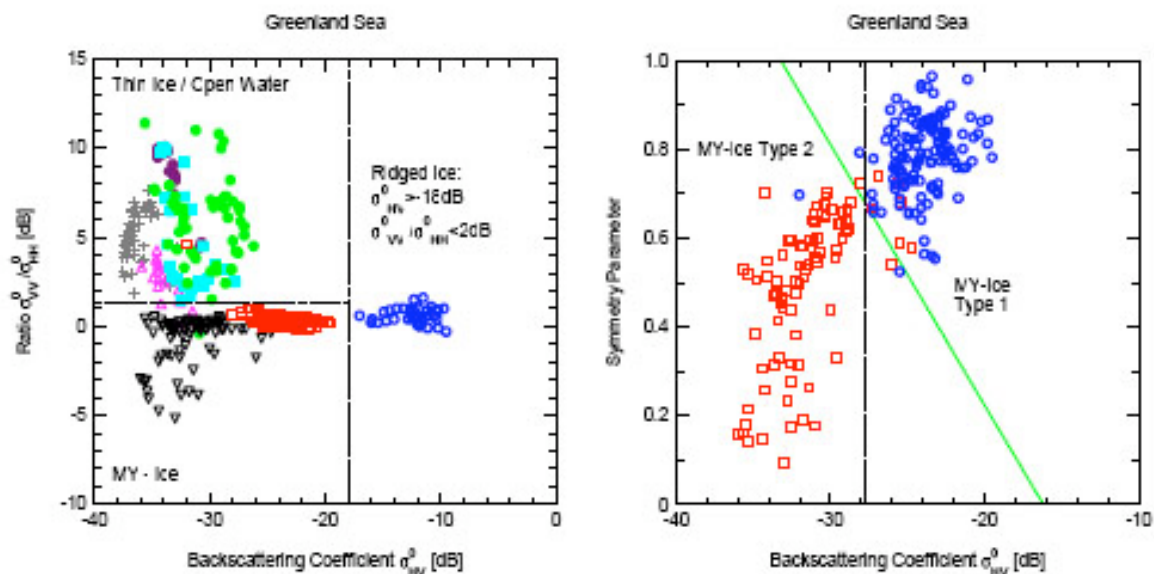
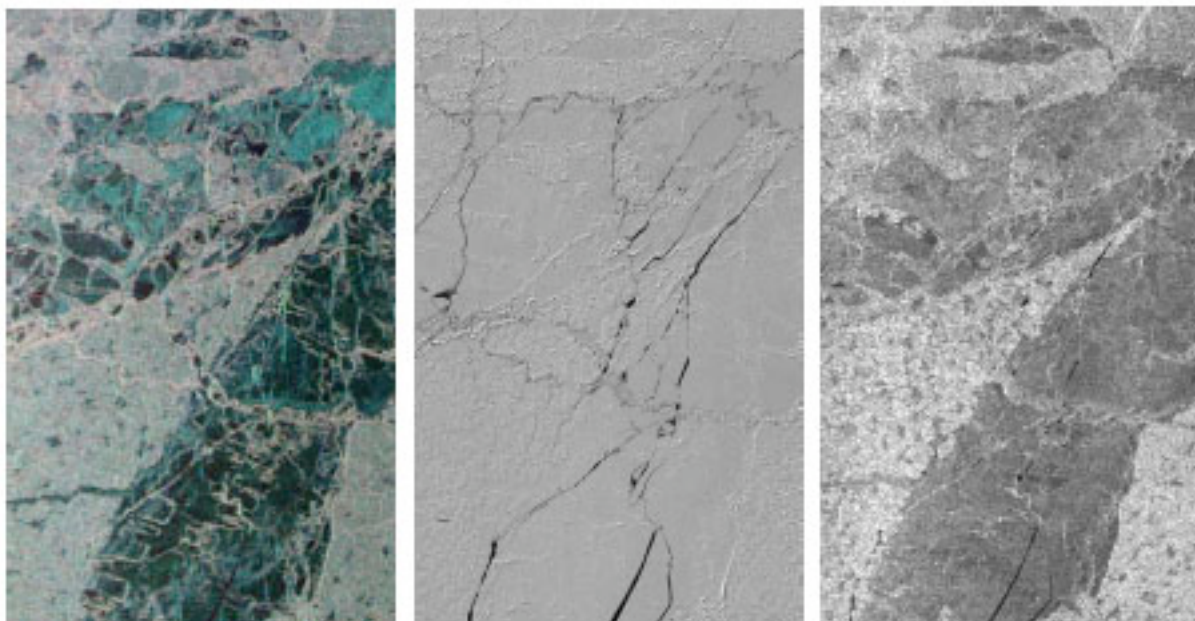


Figure 33. Step 1 (left) and step 2 (right) of a potential classification scheme, developed for the data set from the Greenland Sea. In the left plot, the data marks indicate the following ice classes (listed in terms of colours): blue – ridges, red – MY1, black – MY2, green – TH1 (thin ice), light blue – TH2, pink – TH3, grey – TH4, violet – OW (open water). Ridges can be well separated by the backscattering coefficient at cross-polarisation, MY-ice and thin ice by the co-polarisation ratio. The two species of MY ice can be discriminated by either the backscattering coefficient at HVpolarisation,  $\sigma_{HV}^0$ , or a combination of  $\sigma_{HV}^0$  and the symmetry parameter (Courtesy: W. Dierking).



The ESAR airborne SAR system operated by German Aerospace Center (DLR) Alfred Wegener Institute has been used to carry out sea ice campaigns in the Svalbard area. The most recent campaign took place in March – April 2007 (ICESAR experiment), where the ESAR was operated in L-band polarimetric mode and C-band dual-polarization modes (HV/HH and VH/VV). The main purpose of the ICESAR experiment was to carry out pre-studies for the ESA Sentinel-1 satellite to find optimal SAR configuration for sea ice monitoring (Dierking et al., 2007).

Figure 34 shows example from the SVALEX experiment in 2005, where a L-band 3-layer ESAR image is compared to the corresponding images acquired at X-band VV-polarization and with the optical scanner used on the AWI airplane. The dark green areas in the L-band image are thin ice up to 0.3 m thick (nilas, grey and grey-white ice). These areas correspond to the dark and dark grey patches in the X-band image. Deformation patterns are easier to recognize at L-band. The thin ice areas can be identified at both frequencies using the radar intensity as a classifier, and can hence be excluded when computing parameters characterizing higher roughness elements. The examples in Fig. 34 show the possibilities to map details of the sea ice cover with 3 m resolution SAR images that new SAR satellites will provide, such as ALOS PALSAR, TerraSAR-X, CosmoSkyMed, RADARSAT-2, and Sentinel-1.



*Figure 34. ESAR and linescanner images from SVALEX. Left: L-band, R: cross-polarization, G: HH-, and B: VV-polarization; middle: optical data; right: X-band VV-polarization. The image width corresponds to about 1400 m, the spatial resolution of the radar images is 3 m, of the optical image about 1 m. Courtesy: W. Dierking.*

## **4.2. Ice thickness and roughness from radar altimetry**

A method for ice thickness retrieval from radar altimeters data has been developed by Laxon et al (2003) based on ERS altimeter data which have been obtained up to 81.5°N since 1992. The method is based on separation of the radar altimeter return pulses from sea ice floes and open water or thin ice in leads, and then calculation of freeboard which is

translated into thickness based on climatological estimates of snow cover and ice density. The ice thickness estimates are result of averaging all the data to monthly means values in typically 100 by 100 km grids (Fig. 35).

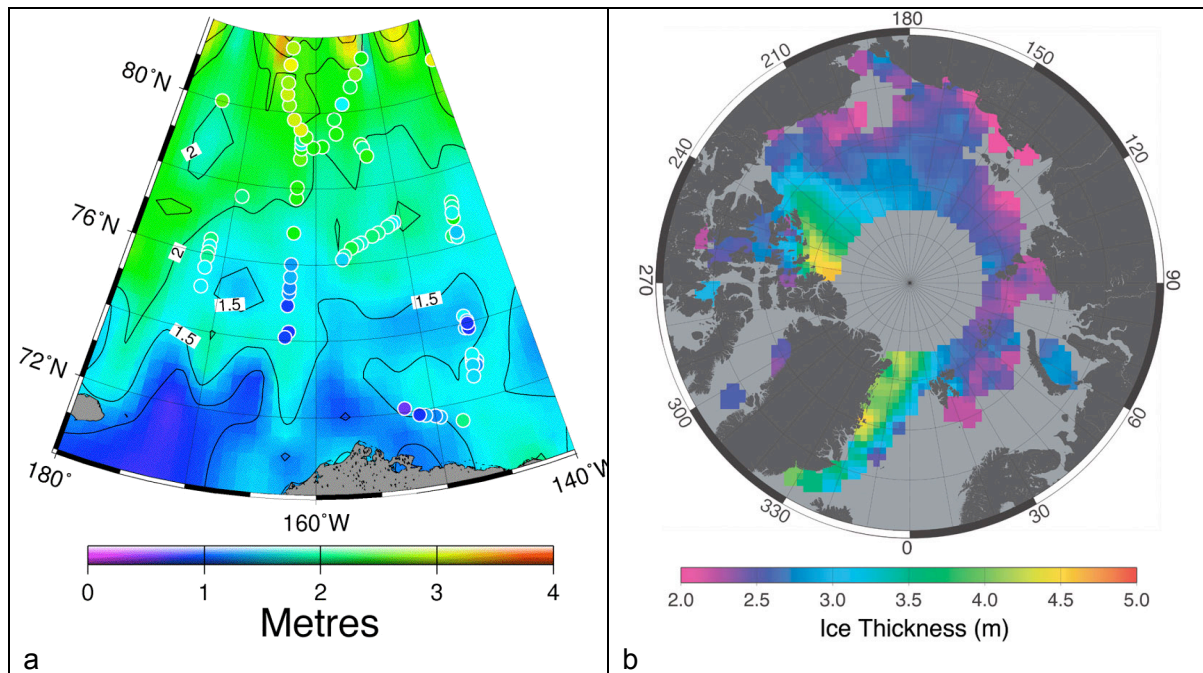


Figure 35. (a) Sea ice thickness map from the Beaufort sea derived from ERS radar altimeter, where the dots represent validation data from submarine sonar profiles; (b) global ice thickness map from radar altimeter. The products have been developed by S. Laxon, Centre for Polar Observation and Modelling, University College London.

This method will be used to retrieve freeboard and ice thickness from CryoSat, scheduled for launch in 2009. This satellite is planned to provide monthly mean ice thickness fields for nearly the whole Arctic for a period of 3 years. The prototype of the beam-limited radar altimeter on CryoSat is the Delay Doppler Phase monopulse (D2P) Radart Altimeter which has been developed at Applied Physics Laboratory at John Hopkins University (Leuschen and Raney, 2005). Several airborne campaigns have been conducted with the D2P altimeter in combination with laser and optical images.

One example of D2P radar and laser profiles over sea ice is shown in Fig. 36, showing data collected at low altitude ( $\approx 250$  m) over a horizontal extent of about 1 km. The white profile near the top shows a profile of the sea ice derived from the laser and radar height values. The labels between the radar response and the sea ice profile divide regions of the image into new ice, open water, and sea ice. New ice is identified by a specular waveform and level tracking. For a typical quasismooth surface, radar energy is backscattered at all angles, but the surface of new ice within a lead is so smooth and level that only near-perfect vertical reflections are generated from the radar's illumination. The resulting specular response consists of the nadir reflection (blue hue), but lacks the usual off-nadir components apparent at later time delays observed in other waveforms. The specular interpretation is also reinforced by a much larger signal power (not apparent in this data format in which all waveforms have been normalized). Open water is identified by a rougher waveform (broader range of hues) and a slightly lower height compared to the new ice. Sea ice is identified by varying waveform roughness and height values.

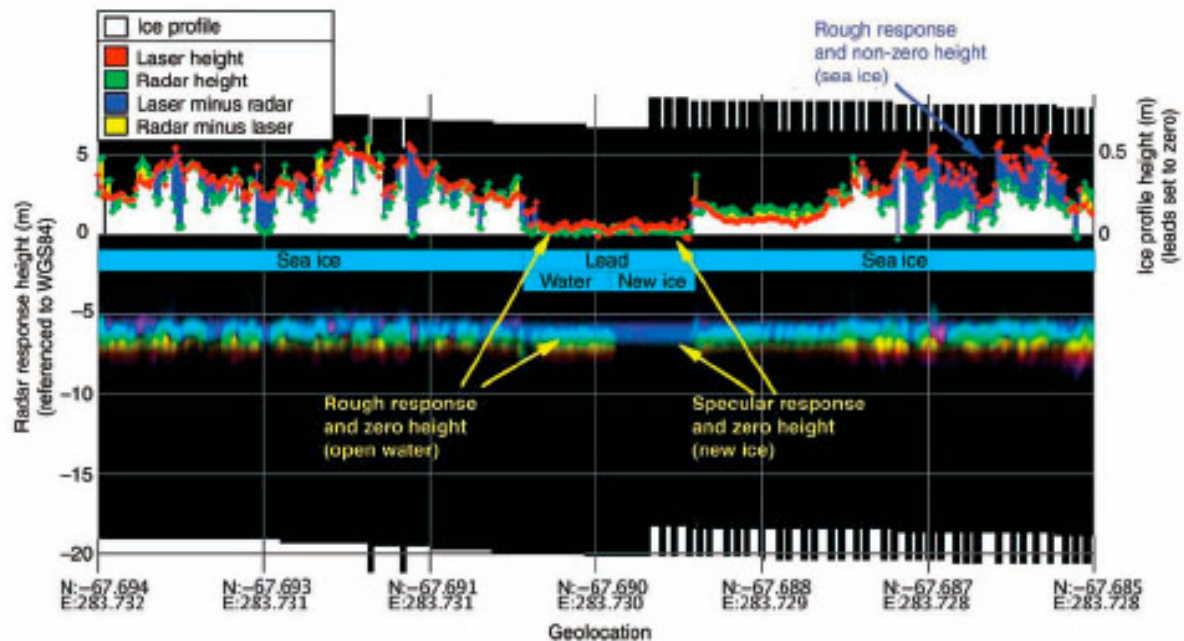


Figure 36. Example data over Antarctic sea ice. A profile of the radar waveforms is shown as a function of height (left axis) and geolocation. The length of the profile is about 1/100 of a degree N-S, corresponding to about 1 km. The image is separated into zones corresponding to sea ice, open water, and new ice. A profile of the ice (derived from the LaRA measurements) is displayed near the top using the scale on the right. Regions where the laser is higher than the radar indicate snow cover (Leuschen and Raney, 2005).

The sea ice also appears to be highly fractured by many smaller leads. The ice profile near the top also shows a comparison between the laser height (red) and the radar height (green). In regions where the laser value is higher, the gap between the two values is blue, while in regions where the radar is higher, the hue tends toward yellow. The blue regions are explained to be snow cover as was illustrated in the previous example. An explanation of the yellow regions is more problematic; a need for more comprehensive geophysical descriptions of the local snow and ice is indicated.

## 5. Conclusions

A review of recent literature has been done to assess the state-of-the-art in using satellite data to observe sea ice ridges and deformation zones. Previous studies show that high-resolution SAR images can identify larger ridges and hummock regions and distinguish them from undeformed ice. High-resolution optical images from satellites such as Landsat and SPOT have not the same capability to detect ridges because optical images are less sensitive to surface roughness compared to SAR.

The most important new results are the possibility to measure the vertical dimension of deformed ice using laser and radar altimetry. IceSat has delivered laser altimeter data since 2003, showing the capability map surface roughness, defined as standard deviation of surface elevation, over most of the Arctic sea ice. These maps provide a large scale view of the the amount and height of ridges across the Arctic Ocean. Individual IceSat profiles can



also map individual ridges when used in combination with SAR. Individual IceSat footprints, with size 75 m and spacing of about 400 m, have been compared with high-resolution airborne scanning laser data, showing good agreement. The resolution of the IceSat data is not good enough to map the topography of individual ridges. For this purpose airborne laser data is the best solution.

In the last 10 - 15 years, several SAR sea ice projects have studied the possibility to map ice ridges by SAR and other remote sensing methods. In the Baltic Sea RADARSAT Fine-resolution images with pixels size of 10 m were obtained in combination with optical images, airborne laser surveys and in situ measurements. The studies showed that SAR can identify ridges and hummocks down to scales of 30 cm, but also other features such as cracks and ship tracks in ice give similar signature in the SAR images. The SAR signals are very sensitive to roughness on scales of a few cm. This means that small-scale roughness due to rubble fields, brash ice or frost flowers on young ice can produce similar backscatter as larger ridges and hummocks. The SAR is a good instrument to detect surface roughness features, but it is not capable of quantifying the size of the roughness features. In order to produce height and width measurement of ridges from remote sensing instruments, it is necessary to use airborne instruments such as scanning lasers and radar altimeters with spatial resolution of 1 m or better.

Airborne radar altimeters have been used in several campaigns to test the capability to measure freeboard and retrieve ice thickness. The delay-Doppler Phase-monopulse (D2P) technique gives the possibility to obtain high-resolution profiles of surface elevation along the flight track. For example, flights with the D2P altimeter in combination with laser altimeters have produced high-resolution profiles across ridges and leads. These are studies in preparation for Cryosat, which will carry a radar altimeter similar to the D2P from 2009.

New SAR systems with polarimetric capability to produce SAR images with resolution down to 3 - 5 m will improve ridge observations. Previous studies with polarimetric SAR from aircraft and space shuttle suggest that use of multi-polarisation SAR will be useful for observation of ice surface topography, but more quantitative studies are needed to find the best methodology. The recently launched TerraSAR-X and Cosmo-SkyMed satellites and RADARSAT-2 scheduled for launch in 2008 will provide both higher resolution and multipolarisation capability.

Regarding high-resolution optical images, there has not been any dedicated studies for detection of ridges, although there are available images with 1 m resolution (e.g. Quikscat). SPOT images, for example, can deliver stereo-photogrammetric products, but these have not been tested for ridge detection. The possibility to map and quantify sea ice ridges with high-resolution satellite data is now better than ever before, but it is necessary to carry out dedicated studies where the new satellite data are explored. Such studies should also include aircraft surveys with scanning laser, radar altimeter and electromagnetic induction sensors to measure the ice draft. A future ice observing system for offshore operations should include both satellite monitoring, aircraft surveys as well as underwater in situ systems in strategic locations.

## References

- Dierking, W., J. Hartmann and C. Lupkes. SVALEX 2005 and ICESAR 2007 – Two flight campaigns over sea ice and land ice in the Svalbard region: Sea ice studies. Proc. 'Envisat Symposium 2007', Montreux, Switzerland, 23-27 April 2007, ESA SP-636, July 2007. (<http://envisat.esa.int/envisatsymposium/>).
- Haas, C., *et al.* (2006). "Comparison of the sea ice thickness distribution in the Lincoln Sea and adjacent Arctic Ocean in 2004 and 2005." *Ann. Glaciol.* **44**.
- Hakkinen, S. (1987). A constitutive law for sea ice and some applications. *Mathematical modelling*, vol. 9, no. 2, pp. 81-90.
- Hvidegaard, S. M. and R. Forsberg. Sea-ice thickness from airborne laser altimetry over the Arctic Ocean north of Greenland. *Geophys. Res. Letter.* Vol. 29n No. 20, pp. 1952, 2002.
- IRIS Final Synthesis Report (2006): Ice Ridging Information for Decision Making in Shipping Operations (available from <http://www.tkk.fi/Units/Ship/Research/Iris/Public/>).
- Johannessen O. M., V. Yu Alexandrov, I. Ye. Frolov, S. Sandven, M. Miles, L. P. Bobylev, L. H. Pettersson, V. G. Smirnov and E. U. Mironov. *Polar Seas Oceanography, Remote Sensing of Sea ice in the Northern Sea Route: Studies and Applications.* Praxis Springer, 2007, 472 pp.
- Kovacs, A. (1971). On pressured sea ice. In: *Sea Ice: Proceedings of an International Conference*, Reykjavik, Iceland, pp. 276-295.
- Kwok, R. (1998) The RADARSAT Geophysical Processor System. In Tsatsoulis and Kwok (eds.) *Analysis of SAR Data of the Polar Oceans*. Springer Verlag, pp. 235 – 257.
- Kwok, R. and G. F. Cunningham. Seasonal ice area and volume production of the Arctic Ocean: November 1996 through April 1997, *J. Geophys. Res.* 107 (C10): art. no. 8038, 2002.
- Kwok, R., H. J. Zwally, and D. Yi (2004), ICESat observations of Arctic sea ice: A first look, *Geophys. Res. Lett.*, 31, L16401, doi:10.1029/2004GL020309.
- Kwok, R., G. F. Cunningham, H. J. Zwally, and D. Yi (2006), ICESat over Arctic sea ice: Interpretation of altimetric and reflectivity profiles, *J. Geophys. Res.*, 111, C06006, doi:10.1029/2005JC003175.
- Laxon, S., N. Peacock and D. Smith (2003) High interannual variability of sea ice thickness in the Arctic region. *Nature*, Vol. 245, pp. 947 – 950
- Maykut, G.A. (1982). Large-scale heat exchange and ice production in the central Arctic. *Journal of Geophysical Research*, vol. 80, no. C8, pp. 7971-7984.
- Melling, H. (1998), Detection of features in first-year pack ice by synthetic aperture radar, *Int. J. Remote Sens.*, 19, 1223– 1240.
- Peterson, I. K., S. J. Prinsenbergh, and J. S. Holladay. 2006. "Comparison of Helicopter-borne Measurements of Sea-Ice Properties with ENVISAT ASAR APP Data for

Amundsen Gulf". in Proceedings of the 2006 IEEE International Geoscience and Remote Sensing Symposium and 27th Canadian Symposium on Remote Sensing Denver, Colorado, July 31 - August 4, 2006.

Pettersson, L. H., S. Sandven, Ø. Dalen, V. V. Melentyev and N. I. Babich. Satellite radar ice monitoring for ice navigation of the ARCDEV tanker convoy in the Kara Sea. Proceedings of The 15<sup>th</sup> International Conference on Port and Ocean Engineering under Arctic Conditions, Helsinki, Finland, August 23 – 27, 1999, pp. 141 - 153.

Rothrock, D.A. (1975). The energetics of the plastic deformation of pack ice by ridging. Journal of Geophysical Research, vol.80, no. 33, pp. 4514-4519.

Sandven, S., M. Lundhaug, Ø. Dalen, K. Kloster and V. Alexandrov. Satellite observations of sea ice in the Bothnian Bay. In *Local Ice Cover Deformation and mesoscale Ice Dynamics* (Ed. Riska and Tuhkuri), *Part 1: Final Scientific Report* from the "Ice State" project funded by EU MAST III. Helsinki University of Technology, Ship Laboratory, M-242, 393 pp, Espoo 1999.

Sandven, S., V. Alexandrov, M. Doble, R. Forsberg, K. Giles, C. Haas, K. Kloster, S. Laxon, J. Lieser, D. Peddie, A. Ridout, H. Sagen, P. Wadhams, and J. Wilkinson. Contract Number: EVK2-CT-2002-00146. SITHOS Final scientific report. NERSC Technical report no. 270, February 2006, 77 pp.

Vesecky, J. F., M. P. Smith, and R. Samadani (1990), Extraction of lead and ridge characteristics from SAR images of sea ice, IEEE Trans. Geosci. Remote Sens., 28(4), 740– 744.

Warren, S. G., I. G. Rigor, N. Untersteiner, V. F. Radionov, N. N. Bryazgin, Y. I. Aleksandrov, and R. Colony (1999), Snow depth on Arctic sea ice, J. Clim., 12(6), 1814– 1829.

### Other relevant references

Bertoia, C., J. Falkingham, and F. Fetterer, *Polar SAR data for operational sea ice mapping*, in: Tsatsoulis, C., and R. Kwok (eds.), *Analysis of SAR data of the polar oceans – Recent advances*, pp. 202-234, Springer, Berlin/Heidelberg/New York, 1998.

Dierking, W., and J. Askne, *Polarimetric L- and C-band SAR signatures of Baltic sea ice observed during EMAC-95*, in: P. Gudmandsen (ed.), 'Future Trends in Remote Sensing', pp. 329-336, Balkema, Rotterdam, 1998.

Dierking, W., Busche, T., Saldern, C. von, Hartmann, J., Haas, C., Luepkes, C., Hajnsek, I., Scheiber, R., Horn, R., Fischer, J., Dall, J.(2006). Sea ice deformation mapping by means of SAR, EUSAR 2006 Conference Proceedings.

Drinkwater, M. R., R. Kwok, D. P. Winebrenner, and E. Rignot, *Multifrequency polarimetric synthetic aperture radar observations of sea ice*, J. Geophys. Res., Vol. 96(C3), pp. 20679-20298, 1991.

Lensu, M. The evolution of ridged ice fields. PhD Thesis, Helsinki University of Technology, Ship Laboratory, M-280, 142 pp, Espoo, June 2003.

Wadhams, P. *Ice in the Ocean*. Gordon and Science Publishers, Amsterdam, 2000, 531 pp.